

RESEARCH ARTICLE | DECEMBER 11 2023

Thermal conductivity of group IV elemental semiconductors

EP FREE

A. V. Inyushkin  

 Check for updates

J. Appl. Phys. 134, 221102 (2023)
<https://doi.org/10.1063/5.0178256>

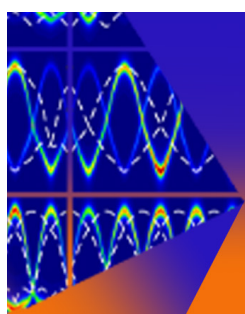


View
Online



Export
Citation

CrossMark



Journal of Applied Physics
Special Topic:
Thermal Transport in 2D Materials

Submit Today

 AIP
Publishing

Thermal conductivity of group IV elemental semiconductors

EP

Cite as: J. Appl. Phys. 134, 221102 (2023); doi: 10.1063/5.0178256

Submitted: 26 September 2023 · Accepted: 18 November 2023 ·

Published Online: 11 December 2023



View Online



Export Citation



CrossMark

A. V. Inyushkin^{a)} 

AFFILIATIONS

National Research Center Kurchatov Institute, Moscow 123182, Russia

^{a)}Author to whom correspondence should be addressed: inyushkin_AV@nrcki.ru

ABSTRACT

The thermal conductivity of group IV elements—germanium, silicon, and diamond—is described in order to demonstrate various important and interesting aspects of the mechanism of phonon heat transfer in single-crystalline semiconductors and dielectrics. The measured temperature dependence of thermal conductivity $\kappa(T)$ for these materials reveals different phonon scattering processes that determine thermal conductivity. In addition to the intrinsic processes of phonon–phonon scattering, scattering by isotopes, dopants, free electrons, sample surfaces, the effects of phonon focusing, irradiation with high-energy particles, and phonon hydrodynamics are discussed.

Published under an exclusive license by AIP Publishing. <https://doi.org/10.1063/5.0178256>

I. INTRODUCTION

Thermal conductivity is one of the most important physical properties of a material, characterizing the ability to conduct thermal energy through its structure. The higher the thermal conductivity value, the faster heat is transferred through the material. The range of thermal conductivity of solids (with zero porosity) is just over 4 orders of magnitude at room temperature, from about $0.1\text{--}0.2 \text{ W m}^{-1} \text{ K}^{-1}$ for plastics to $3150 \text{ W m}^{-1} \text{ K}^{-1}$ for single isotope diamond and higher than $4000 \text{ W m}^{-1} \text{ K}^{-1}$ for suspended isotopically pure ^{12}C (0.01% ^{13}C) graphene at 320 K .¹ The thermal conductivity value of a material in many cases determines its usefulness in many advanced applications. For example, thermoelectric applications, such as solid-state heat-to-electricity conversion and refrigeration, require semiconductor materials with minimal thermal conductivity, while materials with high thermal conductivity are needed to remove heat from local sources in electronic devices. To develop new materials with specified properties, including optimal thermal conductivity, knowledge of the thermal conductivity of solids is necessary.

As Berman has written in his book,² there are several mechanisms that cause heat conduction in solids and many processes that limit the effectiveness of each mechanism. Various collective excitations in solids (quasiparticles—phonons, electrons, magnons, excitons, polarons, etc.), which have a certain momentum \mathbf{q} and energy $E(\mathbf{q})$, can participate in the energy transfer in solids if they have nonzero group velocity $\partial E / \partial \mathbf{q}$. Quasiparticles of the same type (or

one subsystem) interact with each other, with lattice defects, and with quasiparticles of other subsystems. It often turns out to be possible to introduce the concepts of scattering time τ of a given quasiparticle and its mean free path l for various scattering processes.

The main mechanisms of heat transfer in solids are lattice or phonon thermal conductivity κ_{ph} due to thermal vibrations of the crystal lattice and electronic thermal conductivity κ_e . In dielectrics and semiconductors, heat is transferred by phonons; in well-conducting metals, electronic thermal conductivity predominates, and the contribution of phonons turns out to be almost insignificant—as a rule, no more than a few percent; in alloys and poorly conducting metals (semimetals), the electronic and phonon contributions to the total thermal conductivity are comparable. In this Tutorial, we will focus on the thermal conductivity of group IV semiconductors—diamond, silicon, and germanium—the purest single crystals of which provide an example of the phonon mechanism of thermal conduction in perfect crystals with only one type of lattice excitations. From a scientific point of view, studies of the thermal conductivity of these materials have played an important role in the development of basic concepts of the phonon mechanism of thermal conductivity and the development of theories of this phenomenon, both phenomenological^{3–9} and first principles.^{10,11} The latter currently exhibit high accuracy in describing the thermal conductivity of materials and, unlike semi-empirical methods, have predictive power. At present, first-principles

05 January 2024 11:09:57

calculations of phonon thermal conductivity are an actively developing field in the physics of transport phenomena in solids and have become standard practice.^{12–15} The interested reader can find the fundamentals of the theory of thermal conductivity of crystals in the books and reviews mentioned above; pioneering work on the basics of thermal conductivity was described by Klemens.³

The thermal conductivity tensor κ is defined according to the Fourier law as a constant of proportionality between the heat flux \mathbf{Q} and the temperature gradient ∇T ,

$$\mathbf{Q} = -\kappa \nabla T. \quad (1)$$

The most common methods for analyzing phonon thermal conductivity are based on solving the phonon Boltzmann transport equation (BTE) introduced by Peierls¹⁶ in relaxation time approaches.⁷ The thermal conductivity of a crystal is given by^{3,17}

$$\kappa_{\alpha\beta} = \sum_{\lambda} C_{\lambda} v_{\lambda,\alpha} v_{\lambda,\beta} \tau_{\lambda,\beta}, \quad (2)$$

where the summation is over all phonon modes $\lambda \equiv (\mathbf{q}, j)$ with wave vector \mathbf{q} and polarization j ; C_{λ} is the specific heat (per unit volume) of the phonon mode λ ; $v_{\lambda,\alpha}$ is the group velocity of the λ mode along the α direction in a rectangular (Cartesian) coordinate system, and τ_{λ} is the mode lifetime. The total phonon scattering rate τ_{λ}^{-1} is the sum of the rates of all scattering processes in accordance with the Matthiessen rule.

Single crystals of diamond, Si, and Ge have the same *diamond* structure of the face centered cubic lattice with two identical atoms in the base. Being, in general, a tensor of the second rank, the thermal conductivity of these crystals is isotropic and is a scalar quantity,¹⁸ denoted below as κ . This is true when the phonon mean free path is much smaller than the dimensions of the system under consideration. Otherwise, thermal conductivity anisotropy arises, which is determined by the geometry of the sample and its orientation.

II. ABSOLUTE MEASUREMENT OF THERMAL CONDUCTIVITY

A number of methods have been developed for measuring the thermal conductivity of solids.^{19–21} The choice of a specific method is determined by many factors, among which are: the acceptable measurement error, the temperature range of measurements, the mechanical and thermophysical properties of the material under study, and the dimensions of the samples. Apparently, one of the simplest both in concept and implementation is the axial heat flow method,²² which allows, without the use of calibration reference materials, to provide absolute measurements with high accuracy at relatively low temperatures. For measurements, a sample is made in the form of a parallelepiped or a cylinder with a uniform cross section A . A stationary heat flow Q is directed along the sample, creating an axial temperature gradient dT/dx (Fig. 1). For such a one-dimensional case, it follows from Eq. (1) that $Q = P/A$, $dT/dx = \Delta T/L$, and

$$\kappa = -(P/A)L/\Delta T. \quad (3)$$

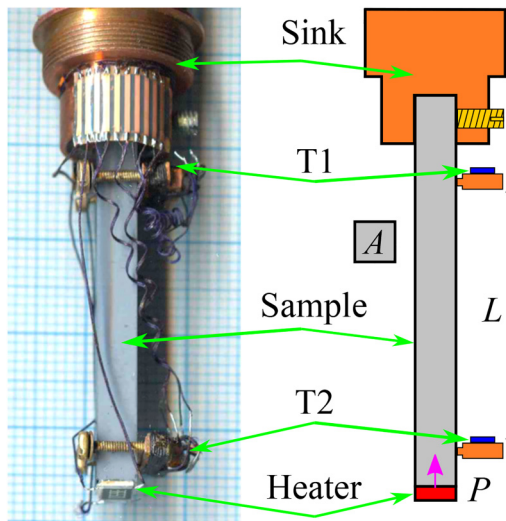


FIG. 1. The left image shows a silicon sample (No. 28SiB100 from Ref. 23) in an experimental cell. The sample measured approximately $4 \times 4 \times 40$ mm³. Schematics for axial heat flow steady state measurements of thermal conductivity is shown on the right. A is the cross section of the sample, L is the distance between thermometers (Cernox CX-1050-SD resistance thermometers), and P is the power generated by the heater (SMD resistor).

05 January 2024 11:09:57

Here, P is the power generated by the heater fixed at the free end of the sample, and L is the distance between two points on the sample, the temperatures T_1 and T_2 of which are measured by thermometers T_1 and T_2 , $\Delta T = T_1 - T_2$. The axial (also called longitudinal) heat flow method allows for accurate measurements with an error of less than 5% for materials with high thermal conductivity at low and moderately high temperatures. To do this, as follows from Eq. (3), it is necessary to accurately determine: (1) the geometry of the sample, (2) the heat flux in the sample that creates the temperature gradient, and (3) the temperature difference between the points of the sample at which the thermometers are fixed.

Determining the dimensions of a sample is usually not a difficult task. The heat power P generated by a resistance heater can also be easily determined by measuring the current flowing through the resistor and the voltage across it. A much more serious experimental challenge is to ensure that this power flows through the sample as an axial flow, at least in the portion of the sample between the thermometer mounting points. Accordingly, it is necessary to create good thermal contact between the heater and the sample and to minimize heat loss from the heater and the sample to the environment to an acceptable level. This is achieved by placing the sample in an evacuated cell with a residual gas pressure of less than 10^{-5} mbar and using electrical wires connected to the heater and resistance thermometers with low thermal conductivity, for example, manganin wires with a diameter of ≤ 0.1 mm and a length of several centimeters. Heat transfer through residual gas and electrical wires is the main source of heat loss at low temperatures, but their contribution to measurement errors can be reduced to less than 1% without much effort.

In addition, there is always heat transfer by thermal radiation from the sample to its environment, which has a lower temperature. The contribution of this heat transfer to the measurement error is negligible at cryogenic temperatures. However, the efficiency of this process increases rapidly with increasing temperature, and, accordingly, the error in determining the value of P increases rapidly. Thus, radiative heat losses become the main source of experimental error in determining the thermal conductivity at relatively high temperatures. In fact, radiative heat transfer limits from above the temperature range of applicability of the axial heat flow method to about several hundred kelvins. The influence of these losses can be significantly reduced by installing radiation shields around the sample being measured and by reducing (if possible) the emissivity of the sample.

Another very important task of the axial flow method is to determine the temperature gradient dT/dx . The objective is to accurately measure a small temperature difference ΔT across a sample (typically $\lesssim 1\%$ of the sample temperature) using thermometers attached to the sample. To achieve the goal, these thermometers should not distort the temperature field in the sample. Adequate technique also includes creating conditions to ensure that thermometer readings correspond to the temperature of the sample at the points where they are attached, i.e., thermometers must be in good thermal contact with the sample, but be thermally insulated from the environment.²³ The thermal boundary resistance between dissimilar materials increases with decreasing temperature²⁴ and can be a big problem in establishing good thermal contact between thermometers and samples at low temperatures.^{25,26} In the case of a sample with a small length and high thermal conductivity (for example, a diamond crystal 4 mm long), it is very difficult to experimentally create a sufficiently large, well-measurable temperature difference across the sample. In this case, even a very small ΔT difference of the order of 1 mK can be accurately measured using a highly sensitive battery of several, for example, ten differential thermocouples^{27–29} at $T > 10$ K.

Also, to achieve precise $\kappa(T)$ measurements, the calibration curve for the resistance thermometer or differential thermocouple that is used to measure the temperature gradient must be sufficiently smooth, as is its derivative.

Other methods are used to accurately measure $\kappa(T)$ at high temperatures, such as the radial heat flow method, in which heat flows from a linear source on the axis of a long cylindrical rod to the outer surface and the temperature difference along the radius is measured. In such a geometry, there is no heat loss by radiation. This method was used by Glassbrener and Slack³⁰ to measure $\kappa(T)$ of Si and Ge crystals at $300 \text{ K} < T < 1600 \text{ K}$. Olson *et al.*³¹ used the flash diffusivity method to determine $\kappa(T)$ of diamonds from 500 to 1200 K. A flash of light generates a thermal pulse on the front side of a plate-shaped sample, which causes a temperature increase on its back side. The dependence of the temperature rise on time gives the thermal diffusivity of the sample. To determine thermal conductivity, additional information about the heat capacity of the sample material is required.

There is a commercial system (Quantum Design PPMS) for measuring $\kappa(T)$ at relatively low temperatures (1.9–390 K), implementing the longitudinal heat flow method in steady-state and pulsed modes.

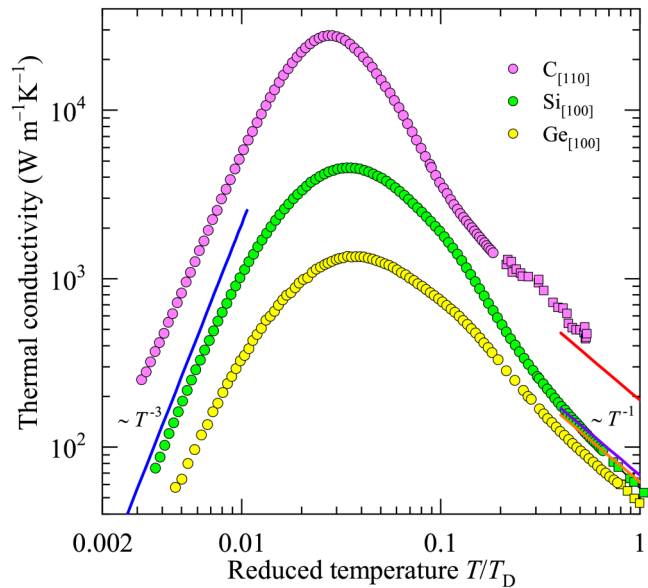


FIG. 2. Thermal conductivity of diamond, Si, and Ge single crystals vs reduced temperature T/T_D . Shown by symbols are the measured data for diamond: sample NE6²⁷ (purple circles) and sample N1³¹ (purple squares); for Si: sample ^{nat}SiA100²³ (green circles) and reference data³³ (green squares); for Ge: sample ^{nat}Ge1(M)³² (yellow circles) and reference data³³ (yellow squares).

05 January 2024 11:09:57

III. THERMAL CONDUCTIVITY AS A FUNCTION OF TEMPERATURE

Figure 2 shows the measured $\kappa(T)$ of high-purity diamond, silicon, and germanium single crystals as a function of reduced temperature T/T_D . Debye temperatures T_D for these crystals are given in Table I. The heat flux \mathbf{Q} was directed along the [110] axis of the diamond crystal²⁷ and along the [100] axis of Si and Ge crystals.^{23,32} Data refer to materials with natural isotopic composition of elements. The graphs are presented in the figure on a double logarithmic scale in order to show clearly the details of the behavior of thermal conductivity when its value changes by several orders of magnitude with temperature.

TABLE I. Crystal parameters and estimated thermal conductivity $\kappa(T_D)$ for group IV elemental semiconductors at the Debye temperature.

Crystal	M_{av}	$V_0 (10^{-24} \text{ cm}^3)$	$T_D (\text{K})^{\text{a}}$	$\kappa (T_D) (\text{W m}^{-1} \text{ K}^{-1})$
C	12.011	5.674	2230	190
Si	28.086	20.024	644	68
Ge	72.640	22.640	374	62

^a $T_D = (6\pi^2 N)^{1/3} (\hbar/k_B)v_D$, where N is the number of atoms of any type per unit volume of the crystal, v_D is the Debye velocity. v_D is determined by averaging over all directions the inverse cube of the phase velocity s_j by numerical integration (j is the phonon polarization); s_j is obtained by solving the Christoffel equations with experimentally determined elastic constants.^{37–39}

At high temperatures, thermal conductivity increases with decreasing temperature. Representing $\kappa(T)$ as a power function $\propto T^{-\zeta}$, we find that $\zeta \approx 1$ near the Debye temperature but increases with decreasing T (in Fig. 2, straight lines represent dependence $\propto T^{-1}$ near $T/T_D = 1$). $\kappa(T)$ changes more strongly with temperature ($\zeta > 1$) at $T \lesssim 0.5 T_D$; the conductivity reaches its maximum value at a temperature T_{\max} of about $0.03 T_D$ and decreases with a further decrease in T . At low temperatures, $\kappa(T)$ follows closely the $\propto T^3$ dependence (represented by the blue straight line in Fig. 2). In the case of diamond, this occurs in the range $(0.005\text{--}0.008) T_D$, and for Si and Ge, at $T < 0.005 T_D$.

Measuring $\kappa(T)$ with sufficiently high accuracy and copiously in temperature points provides valuable information about the processes that limit heat transfer.

IV. ANHARMONIC PHONON-PHONON PROCESSES

Only a few phonon scattering processes determine $\kappa(T)$ of very pure and structurally perfect crystals, with different scattering processes dominating in rather well isolated temperature ranges. At high temperatures, intrinsic phonon-phonon processes, due to the anharmonicity of interatomic bonds, limit the lifetime of thermal phonons and, consequently, the thermal conductivity. Crystals under consideration with a strong interatomic bond, especially in diamond, are weakly anharmonic, and there are no bandgaps between acoustic and optic phonon branches in their phonon spectra. In these crystals, the main role is played by the lowest-order three-phonon processes both without conservation of the total phonon momentum (inelastic Umklapp processes, U-processes) and with conservation of momentum (elastic normal processes, N-processes). Three-phonon scattering leads to the dependence $\kappa(T) \propto T^{-1}$. N-processes are non-resistive in their nature in contrast with U-processes. However, N-processes play a destructive role in thermal conductivity: they enhance a resistive effect of frequency-dependent scattering processes by taking momentum from states, where it is relatively weakly scattered and dumping it to the strongly scattering states.³⁴ Higher-order phonon-phonon processes involving more than three phonons, such as four-phonon processes, decrease $\kappa(T)$ at higher temperatures, resulting in a steeper ($1 < \zeta \leq 2$) dependence on T .

The data presented in Fig. 2 show that $\kappa(T)$ is almost inversely proportional to temperature, which indicates the dominance of three-phonon scattering near T_D . In the case of diamond, the available experimental data have a large scatter at high temperatures and, therefore, do not allow us to draw an unambiguous conclusion about the contribution of four-phonon scattering.

The magnitude of the intrinsic thermal conductivity due to Umklapp three-phonon processes was first treated theoretically by Leibfried and Schlömann.³⁵ They estimated semi-quantitatively the strength of three-phonon processes for face centered cubic crystals having one atom in the unit cell in the high-temperature limit. Subsequently, the formula for $\kappa(T)$ obtained by them was adapted for adamantine (diamond-like) compounds by Slack³⁶ and can be written in the following form:⁹

$$\kappa = A \frac{M_{av} V_0^{1/3} T_D^3}{\gamma^2 n^{2/3} T}, \quad (4)$$

where A is a numerical parameter weakly dependent on γ , M_{av} is the average mass of an atom of the crystal, V_0 is the average volume per atom, γ is the Grüneisen parameter, and n is the number of atoms in the unit cell. For group IV elemental semiconductors having $\gamma \approx 1$ and $n = 2$, parameter $A \approx 3.40 \times 10^{-8} \text{ W cm}^{-2}\text{K}^{-3}$ for M_{av} in atomic mass units u, V_0 in cm^3 , T_D and T in K. From Eq. (4) using the data presented in Table I for the corresponding parameters, one can estimate $\kappa(T)$ at high temperatures. The straight lines in Fig. 2 near $T/T_D = 1$ show these calculated dependencies $\kappa(T/T_D)$. As can be seen, there is a satisfactory agreement between the model results and the experimental data at temperatures near T_D : the theory adequately represents both the temperature dependencies and the values of the measured $\kappa(T/T_D)$ for these three crystals. The Leibfried-Schlömann model gives an approximate estimate of the high-temperature thermal conductivity of materials. In general, this estimate may be far from reality due to a number of simplifications in the interpretation of three-phonon processes (see, for example, Refs. 15 and 40–42).

To accurately determine the anharmonic phonon-phonon processes, it is necessary to calculate the phonon spectrum of the crystal and the phonon damping. To do this, it is necessary to find the numerical values of the interatomic force constants (IFCs), both harmonic (second-order constants) and anharmonic (third and higher orders). Harmonic IFCs allow one to determine the dispersion of phonons. Anharmonic IFCs are related to the phonon relaxation time by Fermi's golden rule. Anharmonicity also leads to frequency shifts in the phonon dispersion, known as phonon renormalization. At present, density functional perturbation theory (DFPT), based on the first-principles approach,⁴³ is used to calculate the IFCs of a crystal. IFC calculations are a rather complex and time-consuming task. In the 1990s, Omini and Sparavigna⁴⁴ pioneered a general iterative solution to the phonon Boltzmann transport equation (BTE). In the 2000s, Broido *et al.*⁴⁵ combined first-principles phonon modeling with an exact numerical (iterative) solution of the BTE and created a reliable *ab initio* approach to calculating the thermal conductivity of materials. The *ab initio* approach gives also a detailed understanding of phonon interaction processes that determine thermal conductivity, such as anharmonic N- and U-processes, involving both acoustic and optical phonons. This approach allows us to take into account the renormalization of the phonon spectrum.

A. N- and U-processes in thermal conductivity

The heat conduction involves phonons with energies of the order of the thermal energy, $k_B T$. At high temperatures $T \sim T_D$, phonon modes with large wave vectors are excited, due to which the U-scattering rate significantly exceeds the N-scattering rate. The difference between N- and U-processes is not important, and N-processes are considered as resistive, along with U-processes. This approximation is called the relaxation time approximation (RTA). As the temperature is lowered, the U-processes quickly "freeze out," while the N-processes do not. As a result, at sufficiently low temperatures, the efficiency of N-scattering prevails over resistive U-scattering, which significantly affects the thermal conductivity. In the case of pure and perfect crystals, when N-processes can play a significant role in the scattering of phonons,

neglecting the non-resistive character of N-processes leads to large errors in thermal conductivity calculations. In the first-principles approach with exact numerical (iterative) solution of the BTE, the approximate solution after the first iteration gives κ_0 , which is the thermal conductivity in the RTA. The conductivity κ_0 is less than κ obtained with the exact solution of BTE.⁴²

In the case of isotopically pure Si and Ge, the room temperature is high, so one can expect relatively strong U-scattering at $T = 300$ K. First-principle calculations indeed show a small difference between κ_0 and κ : κ_0 differs from κ by 2.4% and 6.9% for Si and Ge, respectively.⁴⁶ For diamond with its very high T_D , the room temperature is relatively low, and N-scattering plays an important role: the difference between κ_0 and κ is about 50%.⁴⁶ The specific role of N-processes increases with decreasing temperature as can be seen from Fig. 3, where the ratio κ/κ_0 as a function of temperature is shown for the case of isotopically pure diamond. The ratio increases with decreasing temperature, reaching a value of about 4 at 100 K.

B. Contribution of optical phonons to thermal conductivity

Crystals of diamond, Si and Ge have two atoms in a primitive unit cell. Accordingly, their vibrational spectrum includes optical phonon modes. Since the group velocities of optical phonons are small, their “positive” contribution to the $\kappa(T)$ is also small. However, the presence of a zone of optical phonons in the vibrational spectrum increases the phase space for allowed (by conservation laws) phonon–phonon processes, which increases the efficiency of the phonon–phonon scattering and reduces $\kappa(T)$.⁴⁷ In semiempirical models of thermal conductivity, phonon–phonon processes involving optical phonons are often ignored, which is acceptable at low temperatures, when thermal acoustic phonons

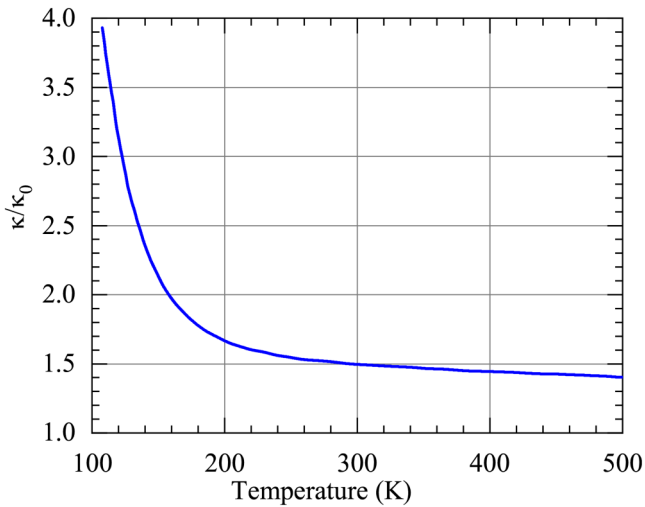


FIG. 3. Ratio of thermal conductivity obtained from the full BTE solution to that from the RTA, κ/κ_0 . Theoretical results are from Ref. 42 for isotopically pure diamond.

dominating in thermal conductivity have energies much lower than optical modes. However, at moderate temperatures, and even more so at high temperatures, for an accurate description of $\kappa(T)$, it is necessary to take into account the features of the phonon spectrum in the entire range of phonon frequencies.

In group IV element semiconductors, the largest contribution to the three-phonon phase space is made by three-phonon scattering involving two acoustic and one optical phonons (ao scattering), as well as three acoustic phonons (aaa scattering). The contribution of aaa processes is less than aao.^{45,47} For example, in Ge, the aao scattering reduces $\kappa(T)$ by about 35% at room temperature.⁴⁸ Figure 4 illustrates the influence of optical phonons on $\kappa(T)$ of diamond and Si. According to calculations, the elimination of aao scattering leads to an increase in the conductivity of diamond and Si by more than 6 and 3 times, respectively, at 300 K. The importance of the aao scattering is a feature of group IV semiconductors. For materials with a large gap between acoustic and optical phonons, aao scattering is very weak and plays a minor role in thermal conductivity, such as in boron arsenide.⁵²

In the case of isotopically pure Si and Ge, acoustic phonons transfer 95% of the heat flux in Si and 92% in Ge at room temperature,⁴⁵ the rest is transferred by optical phonons. Interestingly, the results of first-principles calculations show that optical phonons can contribute over 20% to the thermal conductivity of Si nanowires, i.e., the contribution of optical phonons to conductivity increases in nanostructures compared to bulk materials.⁵³ Also, in some materials, optical phonons have significant dispersion or a higher density of states compared to acoustic phonons so that the

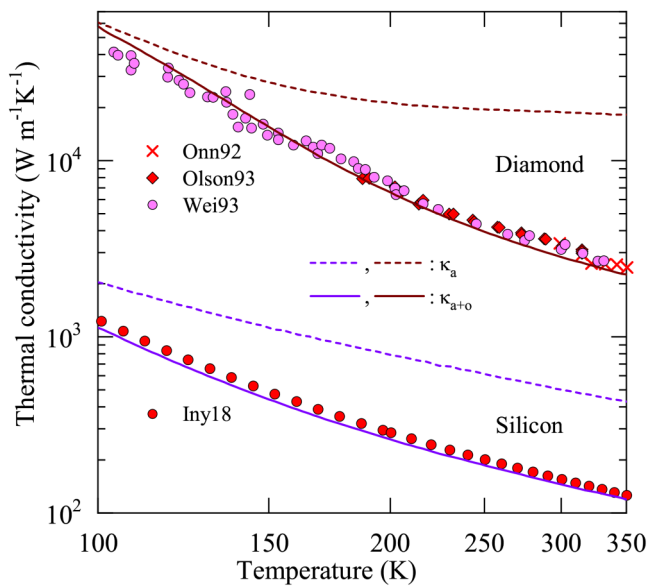


FIG. 4. Thermal conductivity of isotopically enriched diamond and Si from full calculations (solid lines, κ_{a+o}) and for the case when the acoustic-optic channels of phonon–phonon scattering are omitted (dashed lines, κ_a). Experimental data are presented for diamond: Onn92,⁴⁹ Olson93,³¹ Wei93,⁵⁰ and for Si: Iny18.²³ Adapted from Ref. 51.

contribution of optical phonons to thermal conductivity can be large and even dominant, as in bulk hexagonal $\text{Ge}_2\text{Sb}_2\text{Te}_5$.⁵⁴

C. Four-phonon scattering

Lowest-order phonon–phonon processes, namely, three-phonon ones, are the dominant intrinsic processes that determine the phonon damping and $\kappa(T)$ of weakly anharmonic crystals at moderate temperatures and below, where high-frequency phonons are not populated. First-principle calculations of $\kappa(T)$, which properly take into account all the features of three-phonon scattering, confirm this in the case of diamond, Si, and Ge crystals, demonstrating excellent agreement with the measurement results.^{17,55} In principle, the role of higher-order phonon–phonon processes, primarily four-phonon processes, was clear, but it was prohibited to quantify the contribution of such scattering in practice due to the extreme complexity of the problem and the enormous computational costs of its numerical solution. Only recently has the problem of four-phonon scattering of phonons in thermal conductivity been solved and quantitative estimates given.⁵⁶ For group IV semiconductors, four-phonon scattering becomes relatively large and significant at high temperatures.

Figure 5 shows how the inclusion of four-phonon scattering affects the calculated thermal conductivity κ_{3+4} of diamond and Si (an iterative solution of the BTE is implemented).⁵⁵ It can be seen that the three-phonon prediction κ_3 agrees well with the experimental data at relatively low temperatures (<900 K for diamond and <600 K for Si), but at high temperatures a significant deviation is observed, reaching 31% for diamond and 26% for Si at 1000 K.

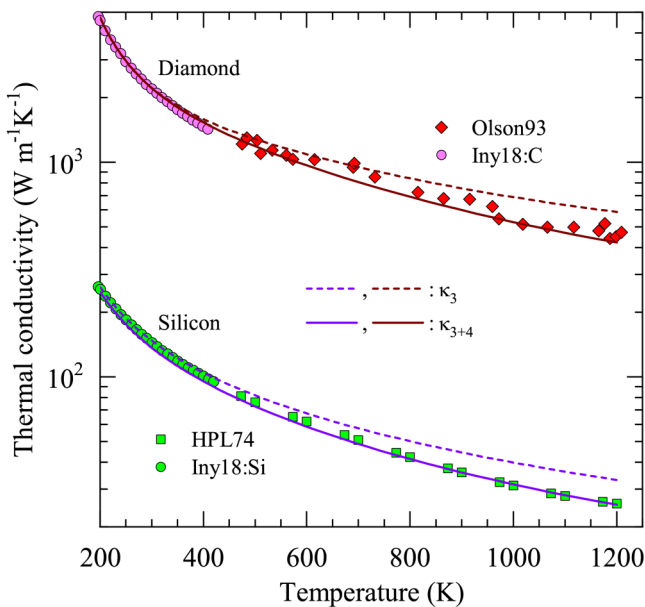


FIG. 5. Thermal conductivities of diamond and Si with natural isotopic abundances. Dashed and solid lines are calculated κ_3 and κ_{3+4} , respectively, from Ref. 55. Symbols represent measured data: Iny18:Si,²³ HPL74,⁵⁷ Iny18:C,²⁷ and Olson93.³¹

Including four-phonon scattering reduces the calculated thermal conductivity at high temperatures, bringing it in excellent agreement with measurements. For Ge, less accurate calculations showed that κ_{3+4} is lower than κ_3 by 15% at room temperature and by 36% at 1000 K.⁵⁸

It should be noted that four-phonon scattering can significantly suppress $\kappa(T)$ of some materials even at room temperature, in contrast to group IV semiconductors. These processes, for example, reduce $\kappa(T)$ of high-thermal-conductivity BAs by approximately 40%⁵⁵ due to the small phase space available for three-phonon scattering.⁵² Also, four-phonon scattering plays a key role in $\kappa(T)$ of strongly anharmonic NaCl¹⁷ and PbTe.⁵⁹ Lindsay *et al.*¹² formulated conditions when four-phonon scattering can play an important role in phonon relaxation: (1) high temperatures, (2) high phonon frequencies, (3) small phase space accessible to three-phonon scattering, and (4) strong anharmonicity of the interatomic potential.

D. Phonon renormalization

The phonon spectrum of a crystal and the damping of phonons, due to the anharmonicity of the interatomic potential, are necessary ingredients in the *ab initio* calculation of the intrinsic thermal conductivity. Phonon modeling is usually based on the perturbative treatment of the anharmonicity of interatomic potentials. This approach is successful for weakly anharmonic solids, including crystals of group IV semiconductors. Moreover, the phonon spectrum is usually calculated in the harmonic (or quasi-harmonic) approximation. Anharmonicity leads not only to phonon damping but also to a shift in phonon frequencies, i.e., to the renormalization of the phonon spectrum. How much does this affect the calculated $\kappa(T)$ of crystals? For diamond, the differences between quasi-harmonic $\kappa_3^{(\text{QH})}$, $\kappa_{3+4}^{(\text{QH})}$ and renormalized $\kappa_3^{(\text{ren})}$, $\kappa_{3+4}^{(\text{ren})}$ are small up to about 400 K¹⁷ (see Fig. 6). For Si, *ab initio* $\kappa(T)$ calculations⁶⁰ show that four-phonon scattering significantly reduces conductivity at $T > 700$ K, and phonon renormalization and thermal expansion (due to temperature-dependent IFCs) have little effect on thermal conductivity.

E. Electronic thermal conductivity

In pure semiconductors at high temperatures, additional thermal conduction channels open, along with the phonon channel, namely, electronic and photonic (or radiative).^{30,61} The photonic contribution for Si and Ge was found to be negligible at all temperatures. Electronic thermal conductivity $\kappa_{\text{el}}(T)$ has two components: electronic polar $\kappa_{\text{el}}^{(p)}(T)$ and bipolar $\kappa_{\text{el}}^{(b)}(T)$ terms: $\kappa_{\text{el}}(T) = \kappa_{\text{el}}^{(p)}(T) + \kappa_{\text{el}}^{(b)}(T)$. The polar term is the usual Wiedemann–Franz contribution produced by free electrons and holes, which predominates, for example, in metals. The bipolar term arises from the bipolar diffusion of electron–hole pairs under the influence of a temperature gradient.

Electronic thermal conductivity $\kappa_{\text{el}}(T)$ was found in both Si and Ge at temperatures above $1.6 T_D$ by Slack and Glassbrenner^{30,61} from analysis of experimental data using semi-empirical models of $\kappa_{\text{ph}}(T)$ and $\kappa_{\text{el}}(T)$. The bipolar term makes the largest contribution to $\kappa_{\text{el}}(T)$, and the polar term makes a small contribution. Both terms, being negligible at $T \sim T_D$,

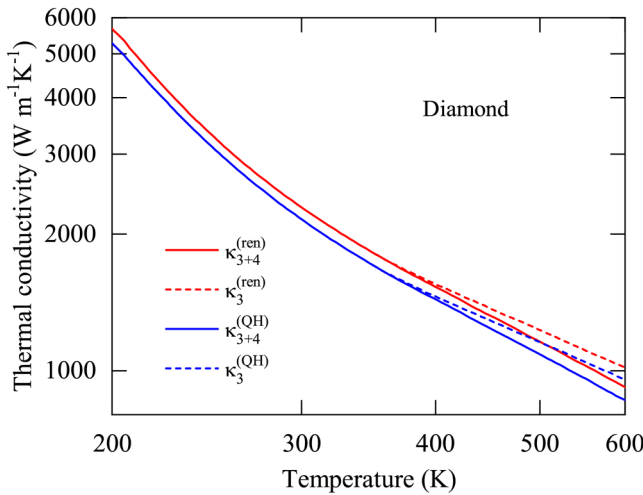


FIG. 6. Theoretical results of Ref. 17 for diamond with natural isotopic composition: 3-phonon (dashed curves) and 3 + 4-phonon (solid curves) limited thermal conductivity with quasiharmonic (blue) and renormalized (red) phonons.

increase significantly with increasing temperature, mainly due to the rapid increase in charge carrier concentration with T . At the melting temperature (1681 K for Si and 1210 K for Ge), the phonon contribution to the sum $\kappa(T)$ is estimated on average to be 51% in Si and Ge, while the bipolar and polar contributions are 32% and 7%, respectively.

Recent first-principles calculations⁶⁰ of the total thermal conductivity of bulk Si, $\kappa_{\text{ph}}(T) + \kappa_{\text{el}}^{(p)}(T) + \kappa_{\text{el}}^{(b)}(T)$, faithfully reproduces the measured data.³⁰ At 1500 K, more than 25% of the heat is transferred by electrons with a predominance of the bipolar term over the polar one by an order of magnitude. The calculation results are in satisfactory agreement with the estimates from Ref. 30.

In the case of diamond, one can expect an even smaller contribution of the $\kappa_{\text{el}}(T)$ to the total thermal conductivity due to the larger gap in the electronic spectrum and the large value of $\kappa_{\text{ph}}(T)$.

F. Why does diamond have the highest thermal conductivity?

Diamond, Si, and Ge show an ordering of the thermal conductivity values according to their Debye temperatures at high temperatures, where phonon-phonon scattering predominates. The other parameters do not affect this order: they are either the same (like n), or approximately the same (like γ), or have little effect (like V_0) on the thermal conductivity for these materials [see Slack's equation (4)].

Phonon thermal conductivity for a number of materials varies inversely with the phase space available for three-phonon scattering, P_3 , in the temperature range where phonon-phonon scattering predominates.^{5,47} This property is completely determined by the phonon dispersion of the crystal. In the case of a known phonon dispersion of a crystal, P_3 can be used for a qualitative assessment

of its thermal conductivity. Among group IV semiconductors, diamond has the smallest value $P_3 = 7.96 \times 10^{-4}$, while Si and Ge have 3.54×10^{-3} and 5.80×10^{-3} , respectively, i.e., 4.4 and 7.3 times more than diamond.⁴⁷ As a result, there are far fewer resistive scattering processes to limit $\kappa(T)$ in diamond.^{51,62} Thus, diamond has the highest $\kappa(T)$ due to the strongest interatomic bonding and lowest atomic mass (resulting in exceptionally high T_D), as well as the very small phase space available to the three-phonon scattering.

The following necessary criteria for a material's high thermal conductivity were established:^{9,36,47}

- High Debye temperature due to small atomic mass M_{av} and strong interatomic bonding ϵ because $T_D \propto (\epsilon/M_{av})^{1/2}$.
- Small Grüneisen parameter due to weak anharmonicity.
- Low number of atoms per primitive unit cell due to simple crystal structure.
- Small phase space available for three-phonon scattering due to specific phonon dispersion.

V. ISOTOPE EFFECTS IN THERMAL CONDUCTIVITY

Group IV elemental semiconductors have several stable isotopes in natural abundance: carbon has two isotopes, ^{12}C and ^{13}C ; silicon—three isotopes, ^{28}Si , ^{29}Si and ^{30}Si ; and germanium—five isotopes with mass numbers 70, 72, 73, 74, and 76. The percentage natural abundance of these isotopes is shown in Fig. 7. The isotopes of an element differ in atomic mass, magnetic and quadrupole moments of nuclei, neutron absorption and scattering cross sections, and other characteristics. The dynamics of the crystal lattice, which determines the phonon thermal conductivity, is itself determined by the interatomic force interaction. The parameters of this interaction are practically independent of the isotopic composition, since the configuration of the electron shell of an atom correlates very weakly with the mass of nucleus M : the scale of this effect is about $m_e/M \sim 10^{-4}$ and m_e is the electron mass. The dependence on the isotopic composition arises because the motion of an atom in the potential created by surrounding atoms depends, among other things, on its mass. Oscillations of atoms at lattice sites can be considered as their motion in a harmonic potential, the parameters of which depend on the volume of the unit cell—the quasi-harmonic approximation. The frequency and the square of the amplitude of atomic oscillations are proportional to $M^{-1/2}$. In thermal conduction, only the mass of the isotope matters. Isotope ("mass") effects can be divided into two types. The first relates the conductivity to the average atomic mass \bar{M} of the chemical element: $\bar{M} = \sum_i c_i M_i$, where c_i and M_i are the concentration and the mass of the i th isotope. The second type refers to the dependence of conductivity on the degree of isotopic disorder. The measure of isotopic disorder is given by

$$g_2 = \sum_i c_i (\Delta M_i / \bar{M})^2, \quad \Delta M_i = M_i - \bar{M}. \quad (5)$$

The values of the isotopic disorder parameter for group IV semiconductors with natural isotopic composition $g_2^{(\text{nat})}$ and with the most disordered composition $g_2^{(\text{max})}$ are presented in Table II. The most disordered mixtures contain 50% of the "extreme" isotopes

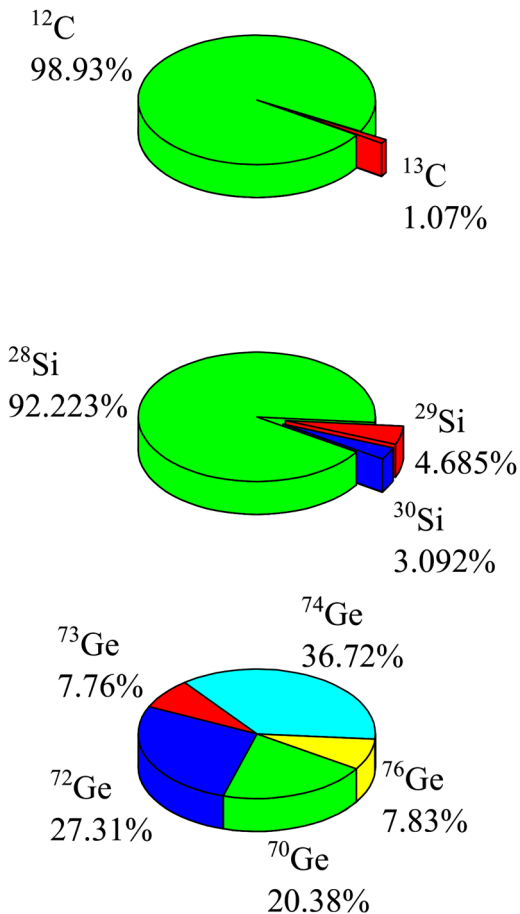


FIG. 7. Natural isotopic composition of C, Si, and Ge.

from the list of isotopes of a given element. It can be seen that $g_2^{(\text{nat})}$ for carbon is approximately 20 times smaller than $g_2^{(\text{max})}$. However, for germanium, the ratio $g_2^{(\text{max})}/g_2^{(\text{nat})} \approx 3$, i.e., its natural composition is relatively close to highly disordered. Silicon has an intermediate disorder.

The mass-disorder effect is not present in isotopically pure and isotopically ordered crystals.

A. Dependence of $\kappa(T)$ on isotopic mass

This isotopic dependence of the phonon thermal conductivity arises due to the trivial transformation of the phonon spectrum with a change in the atomic mass of the lattice. Using Slack's

equation (4), and neglecting the very weak dependence of the atomic volume V_0 and the Grüneisen parameter γ on the mass M of the isotope, we can obtain that $\kappa \propto M^{-1/2}$ at high temperatures. For the elements under consideration, the isotopic masses differ by less than 10%. Hence, the relative change in thermal conductivity with a relative change in the isotopic mass $(\Delta\kappa/\kappa) \approx -1/2(\Delta M/M)$, i.e., a crystal composed of a lighter isotope will have a higher thermal conductivity at a given temperature. This small isotope effect has a linear dependence on $\Delta M/M$.

At very low temperatures, the phonon free path is limited by the size of crystal d and the specific heat of lattice C_v follows the Debye law $\propto T^3$, the thermal conductivity is determined by the formula

$$\kappa \approx \frac{1}{3} C_v v d \propto T^3 / T_D^2 \propto M, \quad (6)$$

where v is the sound velocity. Equation (6) shows that the thermal conductivity increases with the mass of the isotope. Thus, the isotope effect, due to the isotopic transformation of the phonon spectrum, changes sign when going from low to high temperatures.

The isotopic mass effect for silicon⁶³ and germanium⁶⁴ has been studied experimentally. In the case of Si, measurements of $\kappa(T)$ thermal conductivity were performed for two single crystals with a high content of ²⁸Si (99.983%) and ²⁹Si (99.919%) isotopes. It has been found that at low temperatures ($T < 6$ K) in the regime of boundary phonon scattering $\kappa(T)$ for ²⁹Si is higher than for ²⁸Si by 5.6%, which satisfactorily agrees with the calculated 3.6%. At high temperatures, when phonon-phonon scattering predominates, the thermal conductivity of ²⁹Si is lower than that of ²⁸Si by 1.6%, which is very close to the theoretically expected value of 1.8%. The conclusions of the theory of phonon heat conduction on the mass dependence of $\kappa(T)$ semi-quantitatively agree with the experimental results within the relatively large experimental error $\leq 2\%$. In the case of Ge, the measurements of $\kappa(T)$ were performed for three highly enriched single crystals ⁷⁰Ge (99.926%), ⁷²Ge (99.980%), and ⁷⁴Ge (99.921%) at T in the range 80–310 K. Qualitatively similar results were obtained for silicon.

B. Isotope scattering of phonons

In crystals consisting of *poly-isotopic* elements having more than one stable isotope, the isotopes are randomly distributed over the sites of the crystal lattice (with the exception of solid helium at very low temperatures). The mean squares of dynamic displacements of "impurity" isotopes from equilibrium positions differ from the original isotope due to differences in their masses. This creates "dynamic disorder" in the lattice, which leads to temperature-independent *isotope scattering* of phonons already in the harmonic approximation of lattice dynamics. For chemically pure and structurally perfect dielectric crystals, the isotope scattering can play a decisive role in thermal resistivity at low temperatures. This process of thermal resistance was first considered theoretically by Pomeranchuk⁶⁵ in 1942 and experimentally discovered by Geballe and Hull⁶⁶ in germanium in 1958. Dynamic disorder combined with anharmonicity also leads to fluctuating static strain fields around the isotopic impurities.^{67–71} The scattering of

TABLE II. Isotopic disorder parameters for group IV elemental semiconductors.

Crystal	C	Si	Ge
$g_2^{(\text{nat})}, 10^{-6}$	73.9	201	587
$g_2^{(\text{max})}, 10^{-6}$	1600	1200	1700

phonons by such lattice distortions in conventional non-quantum crystals is much smaller than the scattering due to dynamic disorder. However, this isotope scattering mechanism is important in quantum crystals such as solid helium and neon.

For a monatomic crystal of cubic symmetry, the phonon scattering rate due to isotopic mass difference can be represented in the following form:^{6,72}

$$\tau_{\text{iso}}^{-1}(\omega) = g_2 \frac{\pi}{6} V_0 \omega^2 \rho(\omega), \quad (7)$$

where $\rho(\omega)$ is the one-phonon density of states. In the low-frequency limit, when $\rho(\omega) \propto \omega^2$, the Eq. (7) rearranges to a well-known “Rayleigh-type” formula³

$$\tau_{\text{iso}}^{-1}(\omega) = g_2 \frac{1}{4\pi v_D^3} V_0 \omega^4, \quad (8)$$

where v_D denotes the Debye velocity.

Figure 8 shows how isotope scattering affects the thermal conductivity of group IV semiconductors. This figure presents experimental data for bulk single crystals of the highest chemical purity and crystalline perfection to date. The thermal conductivity of highly isotopically enriched crystals demonstrates the intrinsic $\kappa(T)$ of these materials over a wide temperature range. The isotopic compositions of the enriched materials were as follows: >99.95% ¹²C for diamond;⁴⁹ 99.995% ²⁸Si, 0.0046% ²⁹Si, 0.0004% ³⁰Si for silicon sample ²⁸SiA100 and 99.92% ²⁸Si, 0.075% ²⁹Si, 0.005% ³⁰Si for the sample ²⁸SiB100;²³ ≥ 99.99% ⁷⁰Ge, ≤ 0.01% ⁷²Ge for germanium sample ⁷⁰Ge99 and 96.3% ⁷⁰Ge, 2.1% ⁷²Ge, 0.1% ⁷³Ge, 1.2% ⁷⁴Ge, and 0.3% ⁷⁶Ge for the sample ⁷⁰Ge96.^{32,74} At temperatures near T_{\max} of the maximum $\kappa(T)$, the thermal conductivity for isotopically pure Si and Ge is approximately 10 and 8 times greater than for crystals with a natural isotopic content. There are no experimental data on $\kappa(T)$ of isotopically pure diamond crystals at temperatures below about 100 K, at which the maximum $\kappa(T)$ should occur. *Ab initio* models^{75,76} predict that the maximum thermal conductivity of isotopically pure diamond can be an order of magnitude higher than that of ^{nat}C diamond.

The right panels in Fig. 8 show a comparison between measured and *ab initio*-calculated $\kappa(T)$ for crystals with the most isotopically enriched and natural isotopic composition at relatively high temperatures, where $\kappa(T)$ is almost completely determined by anharmonic and isotope scattering. For diamond, $\kappa_{3+4}^{(\text{ren})}$ from Ref. 17 are presented in Fig. 8(d). For Si and Ge, κ_3 from Ref. 46 are shown in Figs. 8(e) and 8(f). *Ab initio* calculations very well reproduce the measured dependencies $\kappa(T)$. In the case of Si and Ge, a slight overestimation of κ_3 over the measured value of $\kappa(T)$ at high temperatures is obviously associated with the neglect of four-phonon scattering in the calculations.

The ratio $\kappa^{(\text{iso})}/\kappa^{(\text{nat})}$ for Si as a function of temperature is shown in Fig. 9. The giant isotope effect near the $\kappa(T)$ peak indicates that it is the scattering of phonons by isotopes that determines $\kappa(T)$ in ^{nat}Si at these temperatures. The same conclusion is valid for Ge and, apparently, for diamond. It is possible that residual impurities significantly limited the measured thermal conductivity

of isotopically pure Si²³ and Ge⁷⁴ near the $\kappa(T)$ peak, despite the very high chemical purity of these crystals.

In addition to the trivial suppression of thermal conductivity by isotope scattering, two important features of $\kappa(T)$ can be distinguished from the experimental data. First, for the most chemically and isotopically pure crystals, the $\kappa(T)$ peak appears as a single narrow peak, rather than, for example, a double peak or a peak with a flat top. Some semi-empirical models, in which the total thermal conductivity is represented as the sum of the contributions of independent longitudinal and transverse phonons, predict just a double peak or a peak with a flat top for perfect crystals. Thus, the experimental data indicate that phonons of different polarizations quite intensively exchange quasi-momenta as a result of the phonon-phonon interaction, forming a single distribution function. Second, an increase in the concentration of impurity isotopes, which are the simplest point defects of the mass-defect type, almost symmetrically suppresses the $\kappa(T)$ peak and only slightly increases the temperature of the maximum. This feature is important in interpreting the observed effects of impurities on $\kappa(T)$ of doped semiconductors (see below).

VI. POINT DEFECT SCATTERING

Point defects in a crystal are atomic-sized defects that cause perturbations in the crystal lattice in their vicinity. Usually, point defects are considered at sufficiently low concentrations, when they do not interact with each other and do not significantly change the lattice dynamics.

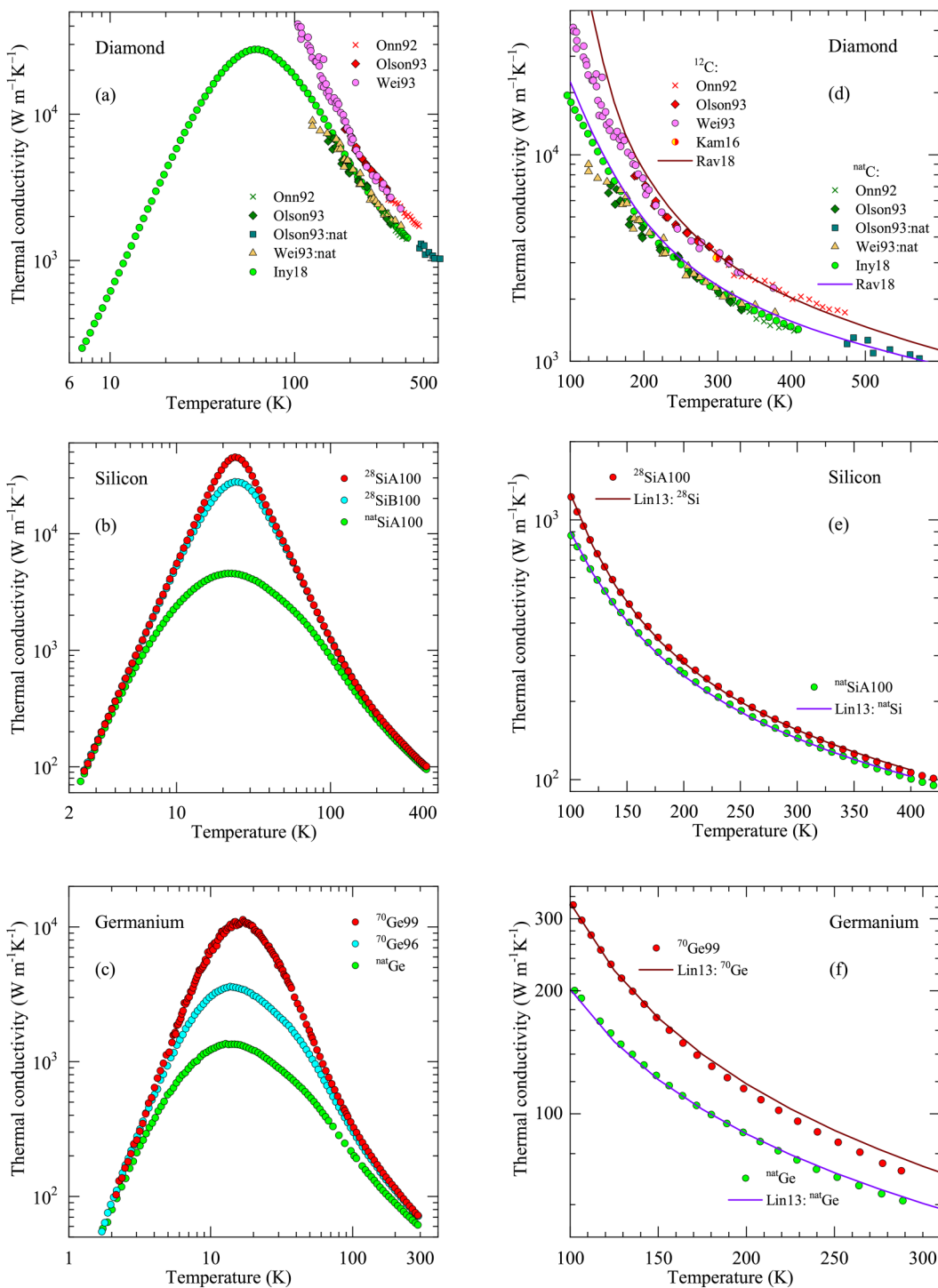
A. Impurity scattering

The effect of the isotopic disorder discussed above is the simplest way to influence the point defects on thermal conductivity. Substitutional impurities have a mass different from the mass of the atoms of the host lattice and cause distortions of the force constants with neighboring atoms and deformation of the lattice in the vicinity of the impurity. The latter changes the force constants due to the anharmonicity of the interatomic potential. All three of these distortions cause phonon scattering by impurities. This scattering can be regarded as a particular but very common case of scattering by point defects. The scattering rate for a cubic crystal in the long wavelength limit can be approximately represented by Eq. (8) with g_2 as a combination of the above three contributions, as shown by Klemens^{3,77} using low-order perturbation theory.

In the absence of reliable information about the perturbed force constants and anharmonicities, the rate of scattering by impurities can be roughly (in order of magnitude) estimated using the expression for the rate of mass-defect (isotope) scattering. A somewhat more accurate estimate is obtained by using Eq. (8) with g_2 given by Turk and Klemens,⁷⁸ which takes into account the change in the atomic volume for an impurity due to a change in interatomic bonds,

$$g_2 = \sum_i c_i \left(\Delta M_i / M + 2\gamma \beta_i \right)^2, \quad (9)$$

where β_i is the fractional volume difference between impurity and host atoms. However, accurate calculation of the rate of point-



05 January 2024 11:09:57

FIG. 8. Thermal conductivity of isotopically enriched and natural isotopic compositions of C (a), Si (b), and Ge (c) depending on temperature, symbols are experimental data. The right panels (d)–(f) show these data and the results of *ab initio* calculations (solid lines) at high temperatures. For diamond, the results of several experiments are presented: Onn92,⁴⁹ Olson93,³¹ Wei93,⁵⁰ Kam16,⁷³ and Iny18.²⁷ The additional tag “nat” denotes a crystal of natural origin, all other crystals were synthetic. Experimental data for Si and Ge are taken from Ref. 23 and Refs. 74 and 32, respectively. Solid lines are theoretical results: Rav18¹⁷ and Lin13.⁴⁶

defect scattering is currently achieved using computational methods, for example, within the framework of Green's function approach^{79–81} or molecular dynamics simulations with interatomic force constants derived from first principles.^{82–84}

B. Impurity nitrogen and vacancy in diamond

In diamonds, nitrogen is the most common impurity presented in different configurations, such as single substitutional nitrogen atom N_s (the so-called “C-center”), two adjacent substitutional nitrogen atoms (A-center), or as an element of nitrogen-vacancy complexes (e.g., NV, NVN, NVH centers, or B-center: four substitutional nitrogen atoms surrounding a vacancy, here “V” stands for vacancy), etc. Most natural stones contain high concentrations of nitrogen, [N] $\gtrsim 2 \times 10^{19} \text{ cm}^{-3}$ (or 100 ppm), in A- and B-centers, and are classified as type Ia. In synthetic crystals, nitrogen atoms present dominantly in C-centers, and these stones are classified as type Ib if the nitrogen concentration is high enough, $> 10^{18} \text{ cm}^{-3}$, and type IIa otherwise.⁸⁵

The experimental data of Berman *et al.*⁸⁶ on the influence of nitrogen impurity on $\kappa(T)$ of natural diamonds are shown in Fig. 10. Experimental data for the purest synthetic diamond from Ref. 27 are also presented for comparison purposes. It can be seen that, at a sufficiently high nitrogen concentration, the $\kappa(T)$ peak acquires an asymmetric shape with a relatively flat left shoulder. A thorough analysis of these and similar experimental data reveal that theoretical models considering nitrogen impurities as only point defects or extended plane defects (so-called platelets) cannot accurately account for $\kappa(T)$ at low temperatures.^{78,86–88}

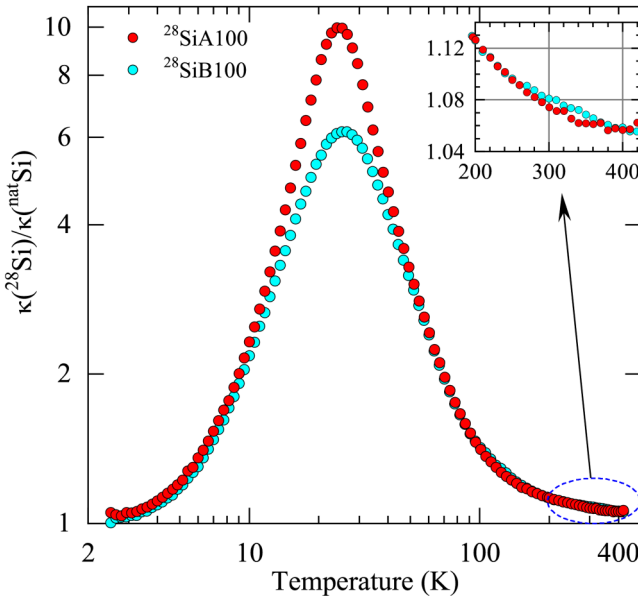


FIG. 9. The ratio of thermal conductivities of enriched crystals of Si to that of crystals with natural isotopic content as a function of temperature. The thermal conductivity corresponds to the direction [100] in the crystal lattice. Adapted from Ref. 23.

Substitutional nitrogen N_s⁰ in the neutral charge state is bonded to four nearest carbon atoms, while the unpaired donor electron is localized on one of the C-N bonds, which leads to an increase in the bond length. This distortion lowers the symmetry of the center from tetrahedral T_d to trigonal C_{3v} due to strong chemical rebonding.⁸⁹ This strong bond perturbation can make a large contribution to the rate of phonon scattering by nitrogen impurities. Katcho *et al.*⁹⁰ validated this by an exact Green's function calculation. If we correlate the contribution S_M of the mass defect with the first term in parentheses of Eq. (9), and the contribution S_K of perturbation of the interatomic forces with the second term, then $S_K/S_M \approx 5$ according to Ref. 90, i.e., somewhat higher than Turk and Klemens' estimate⁷⁸ of about 3.5.

A vacancy is an unoccupied site in a regular crystal lattice. This defect causes a strong perturbation of IFCs in the lattice around itself, which leads to very strong scattering of phonons.⁹⁰ Using Eqs. (8) and (9), it was estimated that the rate of phonon scattering by one vacancy is about 41 times higher than by one nitrogen atom N_s⁰, and the scattering rate by one N_s⁰ is 125 times higher than by one ¹³C atom.²⁹

C. Scattering by neutral and charged impurities

Recently, Fava *et al.*⁹¹ considered the effect of group IV dopants on the thermal conductivity of boron arsenide. Taking into account two types of perturbations due to dopants, on-site mass, and extended bond perturbations, they calculated thermal conductivity from first principles. Phonon-impurity scattering was described using a T-matrix approach,^{79,80} which treats the defects

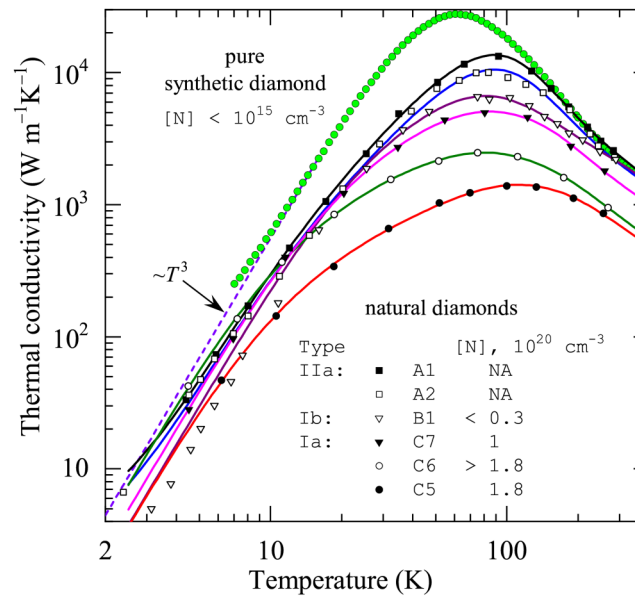


FIG. 10. Thermal conductivity of natural diamonds with different nitrogen content. Symbols represent measurement data from Ref. 86, except for green circles, which are from Ref. 27. NA means that the concentration of nitrogen atoms [N] is not available. Curves are calculated $\kappa(T)$ as described in the text.

05 January 2024 11:06:57

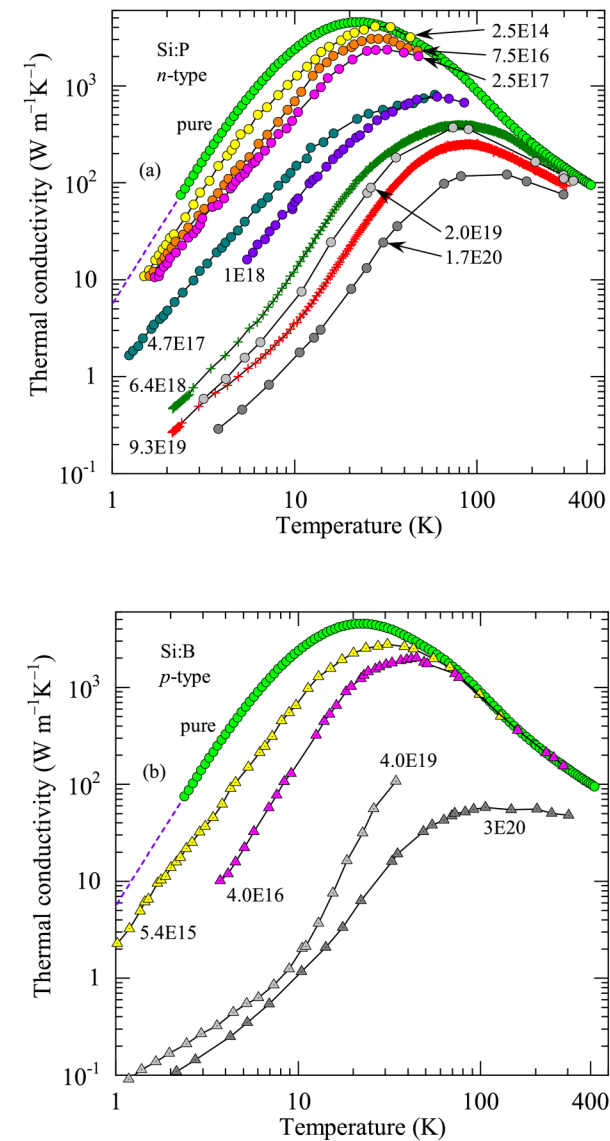


FIG. 11. Thermal conductivity of Si doped with P (a) and B (b). Symbols on panel (a) represent measurement data from Ref. 92 for $[P]$ ranging from 2.5×10^{14} to $1.0 \times 10^{18} \text{ cm}^{-3}$, Ref. 87 for $[P]$ of 2.0×10^{19} and $1.7 \times 10^{20} \text{ cm}^{-3}$, and Ref. 93 for $[P]$ of 6.4×10^{18} and $9.3 \times 10^{19} \text{ cm}^{-3}$. Symbols on panel (b) represent measurement data from Ref. 94 for $[B] = 5.4 \times 10^{15} \text{ cm}^{-3}$, Ref. 95 for $[B] = 4.0 \times 10^{16} \text{ cm}^{-3}$, Ref. 96 for $[B] = 4.0 \times 10^{19} \text{ cm}^{-3}$, and Ref. 87 for $[B] = 3.0 \times 10^{20} \text{ cm}^{-3}$. Data for pure silicon are from Ref. 23. The numbers in the legend indicate the concentration of dopants in units of atoms cm^{-3} . Straight solid lines passing through the symbols serve as a guide for the eyes, and dashed lines represent T^3 extrapolation of $\kappa(T)$ for pure Si.

to all orders in perturbation theory. Through calculations,⁹¹ a general phenomenon was discovered in which charged impurities, isoelectronic with substituted species, scatter phonons noticeably less than their corresponding neutral counterparts. Evidently, the

charge effect is due to different bond perturbations caused by impurities in different charge states and not to a difference in mass perturbations. In charged states, impurities become isoelectronic with the original atom they replaced and more closely match the electronic structure of the host. This results in less bond perturbations and, hence, a lower scattering rate. It would be interesting to investigate this phenomenon in diamond with nitrogen impurities and vacancies.

D. Impurities in silicon

Figure 11 demonstrates $\kappa(T)$ for phosphorus (Si:P) and boron (Si:B) doped silicon. It can be seen that the suppression of $\kappa(T)$ with increasing impurity concentration in the region of the maximum is more symmetrical, and the temperature of the maximum increases only slightly for *n*-type Si:P than for *p*-type Si:B. In addition, boron suppresses $\kappa(T)$ per atom more strongly than phosphorus.

Different impurities have different masses and atomic radii compared to the host atom; therefore, when they are integrated into the host lattice, they cause perturbations of different magnitudes. Lee and Hwang⁸³ investigated the underlying mechanisms for thermal conductivity suppression in Si due to doping: the effects caused by perturbations in mass and interatomic forces, as well as lattice deformation, were evaluated using non-equilibrium molecular dynamics simulations at 300 K. The effect of four substitutional dopants—B, Al, P, and As—was considered. The calculated dependence of the conductivity on the boron concentration at 300 K shows excellent agreement with the existing experimental data, as can be seen from Fig. 12. At a fixed dopant concentration, Al causes the weakest suppression of thermal conductivity, followed by P, B, and As. For clarity, these results are shown in Fig. 13 (bars

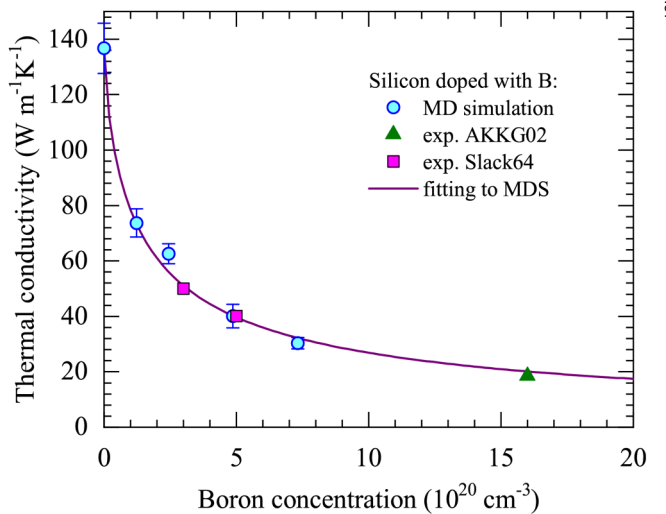


FIG. 12. Calculated thermal conductivity of B-doped Si at 300 K as a function of dopant concentration $[B]$, together with experimental data for comparison. The solid line indicates a fitted curve to the simulation result. Adapted from Ref. 83.

κ_{total}). It also shows how κ of Si is suppressed when only one mechanism of phonon scattering on impurities is taken into account: κ_{mass} is the thermal conductivity of silicon when the mass perturbation is taken into account, and dopant atoms are considered to have the same radius and force constants as Si; κ_{bond} —only the disorder of atomic bonds is taken into account, and the mass and radius of the doping impurity are considered to be the same as those of the Si atom; and, finally, κ_{strain} is the conductivity when only the lattice deformation near the dopant is taken into account, and the remaining parameters are considered unchanged. The calculations show that the mass perturbation is primarily responsible for the κ suppression in the As- and B-doped silicon, whereas the bond perturbation is found to be more important than the mass perturbation in the Si:Al and Si:P; for all these systems, the lattice strain effect turns out to play a minor role in the reduction of thermal conductivity. These results are qualitatively clear, since in the first two cases, the mass difference Δm is large, about 75 and 17 u for As and B, respectively, while in the last two cases, Δm is much smaller, about 1 and 3 u for Al and P.

E. Impurities in germanium

For single crystals of Ge, the different experiments^{30,64,97,98} testified that the change of electrical resistivity within 3–50 $\Omega \text{ cm}$, which corresponds to carrier concentration in the range from 2×10^{12} to $1.5 \times 10^{15} \text{ cm}^{-3}$, does not affect $\kappa(T)$ within experimental error of 5% at $T < 400 \text{ K}$. It is very likely that $\kappa(T)$ is insensitive to impurities with these concentrations even at higher temperatures. At higher concentrations, impurities significantly reduce $\kappa(T)$ of Ge. Measurements show that the magnitude of the effect varies with temperature and depends on the nature of the impurity. For isovalent impurities, it can be expected that impurity

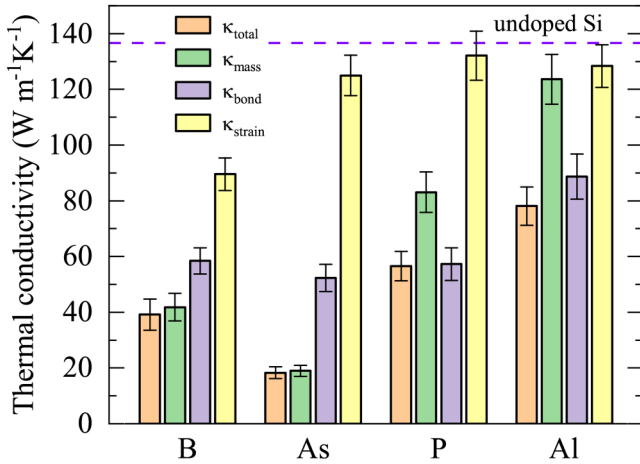


FIG. 13. Calculated thermal conductivities for Si doped with B, As, P, and Al at $T = 300 \text{ K}$ and doping level of $4.875 \times 10^{20} \text{ cm}^{-3}$. The dashed horizontal line indicates the predicted value of κ , $136.65 \text{ W m}^{-1} \text{ K}^{-1}$, for undoped Si. For each doped system, besides its bulk value (indicated as κ_{total}), the κ values calculated by isolating each of the effects of mass disorder (κ_{mass}), bond disorder (κ_{bond}), and lattice strain (κ_{strain}) are also plotted. Adapted from Ref. 83.

phonon scattering is due to local perturbations of the mass, coupling, and lattice strain induced by the impurity. Then, one can expect that the corresponding decrease in $\kappa(T)$ will be qualitatively similar to the decrease caused by impurity isotopes. Figure 14 shows this effect on the example of excess thermal resistivity $\Delta W_{\text{imp}} = 1/\kappa_{\text{imp}} - 1/\kappa_{\text{pure}}$ caused by isovalent Si and Sn impurities in germanium as a function of temperature in the range from 80 to 400 K. This figure also shows the excess thermal resistance ΔW_{imp} in ${}^{\text{nat}}\text{Ge}$ compared to isotopically pure ${}^{70}\text{Ge}$ calculated from first principles. There is indeed a similarity: in both cases, $\Delta W_{\text{imp}}(T)$ rises sublinearly with temperature. However, in the case of the Al acceptor, the behavior of $\Delta W_{\text{imp}}(T)$ differs qualitatively from that considered above: the excess resistivity slightly decreases with temperature. This result indicates the presence in semiconductors with electrically active impurities of an additional specific process of phonon scattering, which acts along with the usual Rayleigh-type point-defect scattering. Note that all three impurities create almost the same mass perturbation in the silicon lattice. This suggests that the difference in the rates of point-defect scattering on these impurities is primarily due to the difference in their interatomic bonds.

The strongest suppression of $\kappa(T)$ in doped semiconductors is observed on the low-temperature side of the maximum. Even at very low concentrations of neutral dopants (less than 10^{16} cm^{-3} for a donor impurity in Ge), the effect can be very strong. Despite a direct correlation between the $\Delta W_{\text{imp}}(T)$ due to an impurity and its concentration, the effect cannot be explained using the usual process of phonon scattering by point defects along with scattering at crystal boundaries. The magnitude of the suppression of thermal

05 January 2024 11:03:57

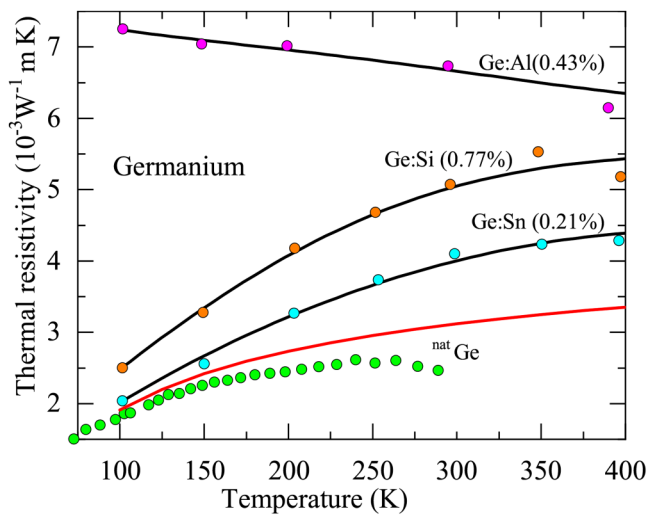


FIG. 14. Excess thermal resistivity of germanium containing Si, Sn, and Al impurities. The concentration of impurities is given in at %. Symbols (magenta, orange, and cyan circles) are experimental data from Ref. 98, and black lines passing through the symbols serve as a guide for the eyes. Green circles represent the calculated ΔW_{imp} caused by impurity isotopes in ${}^{\text{nat}}\text{Ge}$ using the experimental data from Ref. 32 and 74, and the red line are determined from the results of *ab initio* calculations of Ref. 46.

conductivity, the temperature range in which it occurs, depends on the nature of the dopant, its charge state, and concentration. The scattering process that explains many of the observed features of $\kappa(T)$ in doped semiconductors is the scattering of phonons by charge carriers.

VII. PHONON SCATTERING BY CHARGE CARRIERS

Experimental studies of the excess thermal resistance ΔW_{ep} of Ge^{99–101} due to electron–phonon scattering, depending on the concentration of dopants, revealed three concentration regions:¹⁰² (1) a region of low concentration, in which charge carriers are bound to individual dopants, the dopants do not interact because they are located in the lattice at a sufficiently large distance from each other, the system is considered non-metallic; (2) a region of high concentration, in which impurity levels merge with the conduction (or valence) band, charge carriers are free to move about the crystal lattice, as in metals; (3) the region of intermediate concentration, in which the transition from non-metallic to metallic state takes place.

A. Bound charge scattering

The mechanism of phonon scattering by electrons bound to donors was described by Keyes¹⁰³ in 1961 using *n*-type Ge as an example. To simplify the consideration, the hydrogenic model of the donor impurity is used. Ge has four equivalent valleys in the conduction band, so the ground state (*s*-state) of the donor is four-fold degenerate (in diamond and Si, the degeneracy of the ground

state of the donor is sixfold). The spin–orbit interaction and central-cell corrections^{104,105} partly lift the degeneracy and cause a species-dependent splitting of the ground states of the donor¹⁰⁶ into singlet $1s(A_1)$ and triplet states $1s(T_2)$ separated by the energy Δ . Following Keyes's reasoning,¹⁰³ the perturbation of the Ge band structure by a shear strain produces matrix elements of order $\Xi_u \epsilon$ between the singlet state and the triplet states, where Ξ_u is the shear deformation potential constant, and ϵ is the magnitude of the strain in the vicinity of the donor. In the second-order Born approximation, these matrix elements give rise to a term of order $(\Xi_u \epsilon)^2 / \Delta$ in the dependence of the energy of a state on the strain. Phonon scattering arises from virtual transitions of electrons between the donor singlet and triplet levels. The rate of scattering of phonons by bound carriers is several orders of magnitude greater than the rate of scattering by donors as point defects due to the mass and interatomic bond perturbations. The high rate of phonon scattering by bound carriers is associated with a large effect of strain on the energy of an electron bound to a donor. A similar mechanism is applicable to the scattering of phonons by holes bound to acceptors. Note that the rate of scattering of phonons by bound carriers is proportional to the fourth power of the corresponding deformation potential constant, and for low-frequency phonons with $\hbar\omega \ll \Delta$, the rate is proportional to the $1/(\Delta)^2$. That is, an impurity with a small value of splitting Δ will have a scattering rate of low-frequency phonons higher than an impurity with a large splitting, all other parameters being equal. This will lead to a lower $\kappa(T)$ in the case of small splitting. The experimental data of Bird and Pearlman¹⁰⁷ on $\kappa(T)$ for *n*-type Ge doped with donors Sb, As, and P in approximately equal concentrations of electrons bound to donor atoms at low temperatures n_{ex} demonstrate such a dependence at low temperatures (see Fig. 15).

Three types of bound electron scattering have been classified: elastic, inelastic, and thermally assisted phonon absorption.¹⁰⁸ Usually, elastic scattering is the most detrimental for heat conduction. The scattering rate is dopant species dependent and can be represented by the following expression:

$$\tau_{\text{be}}^{-1}(\omega) = N_{\text{nd}} \Xi_u^4 \omega^4 G(\omega, a_B^*, \Delta), \quad (10)$$

where N_{nd} is the concentration of neutral donors and $G(\omega, a_B^*, \Delta)$ is a rather complex function of the phonon frequency, which depends on the effective Bohr radius a_B^* of the bound state and the splitting Δ . The rate $\tau_{\text{be}}^{-1} \sim \omega^4$ for low enough ω and can be orders of magnitude stronger than the mass- and bond-perturbation Rayleigh scattering from the dopant. The bound electron scattering is only effective for phonons with wavelength λ long compared to the a_B^* ; for shorter wavelengths, the donor state cannot be considered as a point defect. Scattering by bound electrons vanishes for short-wavelength phonons, since the strain value averaged over the electron wave function decreases very rapidly as λ decreases below the crossover wavelength $\lambda_{\text{co}} = 2 a_B^*$ or higher the corresponding cut-off frequency ω_{co} . Thus, there is a range of phonon frequencies above the ω_{co} in which the $\tau_{\text{be}}^{-1}(\omega)$ is a rapidly decreasing function of ω . Further, since heat is transferred mainly by phonons with thermal energies $\gtrsim 1 k_B T$, we can estimate in order of magnitude the temperature T_{co} , above which scattering by bound electrons does not affect $\kappa(T)$ or, in other words, vanishes. It is easy to show

January 2024 110957

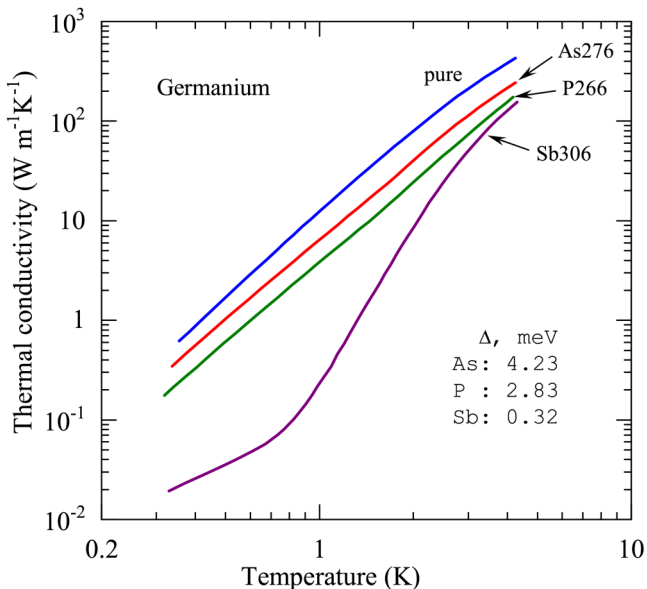


FIG. 15. Thermal conductivity of germanium doped with Sb, As, and P. Experimental data are from Ref. 107. The number of electrons bound to donor atoms at low temperatures is indicated by the number following the atom symbol: As276 means 2.7×10^{16} As/cm³, P266 means 2.6×10^{16} P/cm³, and Sb306 means 3.0×10^{16} P/cm³.

that $T_{co} \sim \pi \hbar v_D / (k_B a_B^*)$. Obviously, the smaller the a_B^* , the higher the temperature T_{co} at which scattering by bound charges manifests itself in thermal conductivity.

At low temperatures, in the case of a significant influence of internal strains on the ground state of dopants, the theory that takes into account elastic and inelastic channels of scattering on bound charges underestimates phonon scattering. The observed strong scattering of low-frequency phonons can be explained by taking into account the resonant absorption of phonons between the dopant ground state, randomly split by internal strains, as demonstrated for Ge¹⁰⁹ and Si.¹¹⁰

It should be noted that the phonon scattering off bound electron (hole) occurs due to the interaction of phonons with the electron (hole) and not with the donor (acceptor) ion itself.^{99,107} Donors that have donated their extra valence electrons lose their ability to scatter phonons by the mechanism of bound electrons, and the thermal conductivity increases. In a semiconductor containing both donors and acceptors, only neutral dopants provide the process of phonon scattering by bound charge carriers. As a result, for compensated semiconductors, the thermal conductivity is higher than for noncompensated semiconductors with a much lower dopant concentration at low temperatures. This effect was investigated in detail by Goff *et al.*^{99,100,111} in Ge doped with various electrically active impurities.

The concentration dependence of the ΔW_{ep} of Ge at $T = 2$ K, constructed from experimental data from Refs. 99, 100, 107, and 111, is shown in Fig. 16. The excess resistance increases with increasing donor content. Two areas of concentration are clearly visible here, differing in the rate of change of ΔW_{ep} from n_{ex} : the area of low concentration, where ΔW_{ep} is roughly proportional to

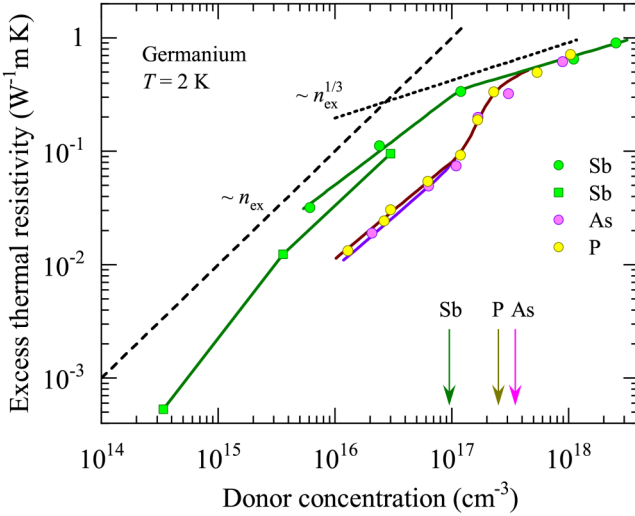


FIG. 16. Excess thermal resistivity of germanium doped with Sb, As, and P, depending on the content of donors. Green and magenta circles are experimental data from Ref. 99, yellow circles are from Ref. 100, and green squares are from Ref. 107; lines passing through the symbols serve as a guide for the eyes. Arrows indicate the values of $n_c^{(exp)}$ for donors.¹¹²

n_{ex} and a region of high concentration with $\Delta W_{ep} \sim n_{ex}^{1/3}$. The excess resistance does not depend on the type of impurity or compensation at a high donor concentration.¹⁰⁰ The region of high concentration starts from about $1 \times 10^{17} \text{ cm}^{-3}$ for Ge:Sb and $4 \times 10^{17} \text{ cm}^{-3}$ for Ge:P and Ge:As. These values almost coincide with the critical concentrations $n_c^{(exp)}$ for the metal-insulator transition in Ge doped with corresponding donors obtained from other experiments unrelated to thermal conductivity.¹¹² The values $n_c^{(exp)}$ are marked with arrows in Fig. 16. Recall the Mott criterion for the metal-insulator transition: $n_c = (x/a_B^*)^3$, $x = 0.2-0.25$ (empirical value), and $x_{Mott} = 0.25$. Since the effective Bohr radius of donors in Si is more than two times smaller than in Ge, the critical concentration of the metal-insulator transition is an order of magnitude higher for Si.¹¹³ Between the areas of low and high concentration, there is an area of intermediate concentrations.

The theory of phonon scattering by bound charge carriers was proposed by Suzuki and Mikoshiba and applied to doped Si and Ge.¹¹⁴⁻¹¹⁶ It satisfactorily reproduces the main features of thermal conductivity due to the scattering by bound charges and was used for analysis of experimental data in a number of works, including studies of $\kappa(T)$ for lightly doped Ge, Si, and diamond.

As an example, let us compare the result of calculating the thermal conductivity $\kappa(T)$ for Si:P in the framework of the phenomenological theory of Callaway with the experimental data of Fortier and Suzuki,⁹² which are presented above in Fig. 11(a). The calculations were carried out taking into account only the elastic scattering of phonons by bound electrons using the simplified Suzuki-Mikoshiba expression for $\tau_{be}^{-1}(\omega)$. It was assumed that

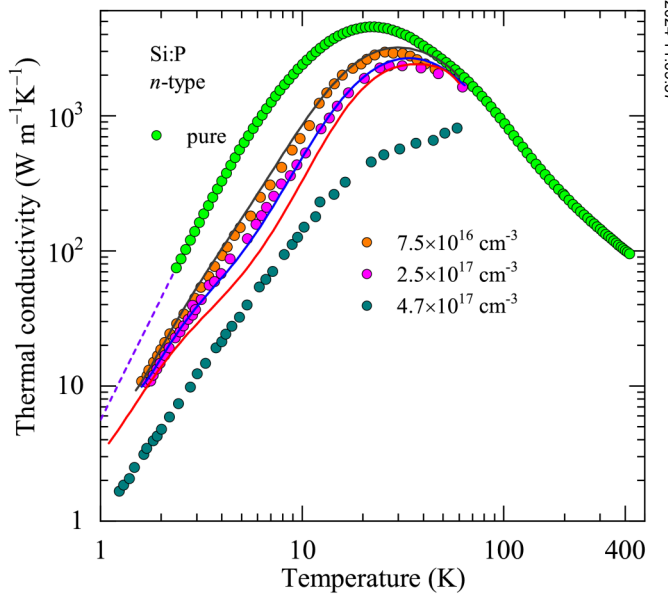


FIG. 17. Experimental (symbols) and calculated (solid lines) $\kappa(T)$ of Si:P data are from Ref. 92; data for pure silicon are from Ref. 23. Dashed lines represent T^3 extrapolation of $\kappa(T)$ for pure Si. The numbers in the legend indicate the concentration of P.

$\Delta = 152$ K, $a_B^{*(P)} = 17$ Å, and $\Xi_u = 10$ eV. With such a large value of Δ , scattering by bound electrons is relatively weak at temperatures of the experiment, below 50 K. The results are shown in Fig. 17. As can be seen, the theory satisfactorily agrees with the experimental data in the region of low P-donor concentration: only the overestimated theoretical $\kappa(T)$ at temperatures near and above the peak attracts attention. For the sample with a relatively high [P] of 4.7×10^{17} cm⁻³, the calculated $\kappa(T)$ cannot reproduce the experimental data. At this concentration, the donor centers apparently interact with each other; this significantly changes the electronic states of the valence shell of phosphorus.

The change in the $\kappa(T)$ of natural diamond with a change in the concentration of impurity nitrogen is shown in Fig. 10 above. Modeling of $\kappa(T)$ for these samples using the Callaway theory, taking into account scattering by point defects of Rayleigh-type and taking into account the elastic scattering of phonons by bound charge carriers, gave a good approximation to the measured data.²⁹ Note that the concentration of nitrogen (and other defects) is not exactly known for these samples. Also, defects that are responsible for scattering by bound carriers are not known. Because of this, the parameters of the scattering rates by point defects and bound carriers were adjustable parameters in the simulation. The authors of Ref. 29 argued that impurity nitrogen, which was present in the samples mainly in the form of A-aggregates, did not create scattering by bound carriers, this scattering is probably due to some other nitrogen-containing defects.

In synthetic diamonds grown by chemical vapor deposition (CVD) and high pressure and high temperature (HPHT) methods, impurity nitrogen is present predominantly in the form of single substitutional nitrogen atoms N_s, unless they have not been subjected to high temperature annealing. However, nitrogen can also be present in CVD diamonds in the form of complexes, for example, NV, NVH, and others, the concentration of which, however, is substantially lower than that of N_s. Doping CVD diamond with N_s leads to suppression of $\kappa(T)$ at relatively low temperatures, which manifests itself in a pronounced dip in $\kappa(T)$ on the low-temperature side of the peak, even at a concentration of about 3 ppm. However, such doping did not affect the thermal conductivity at temperatures near and above room temperature.²⁹ The Callaway model, which takes into account scattering by bound charge carriers, approximated the experimental data very well, as can be seen in Fig. 18. Also shown here is $\kappa(T)$ for a pure CVD crystal. It has a smaller effective diameter, so its $\kappa(T)$ is lower than that of the N-doped sample at the lowest temperatures. However, the effective diameter has almost no effect on $\kappa(T)$ on the high-temperature side of the maximum, so here we can use the experimental data for a pure sample for comparison. The dashed line in Fig. 18 shows the model dependence $\kappa(T)$ for the N-doped sample, without taking into account bound charge scattering. Comparison of the solid curve for the N-doped sample with this dashed curve makes it possible to evaluate the effect of bound charge scattering on $\kappa(T)$ of this diamond sample. It is seen that at temperatures below 120 K, $\kappa(T)$ is strongly affected by phonon scattering on charge carriers bound to the nitrogen-related doping centers. This scattering reduces the value of $\kappa(T)$ by a factor of 2.7 at $T \approx 40$ K. At temperatures below about 6 K, this scattering is ineffective.

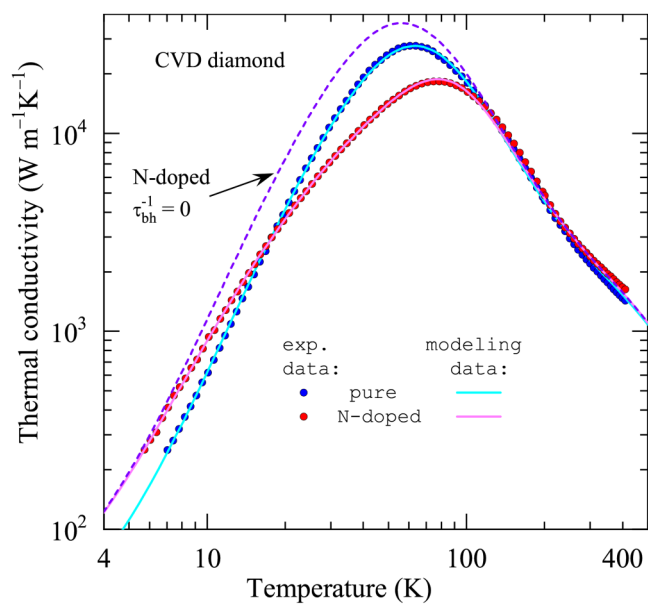


FIG. 18. Thermal conductivity of CVD diamond: experimental (symbols) and theoretical (lines) data for pure and N-doped samples. The solid lines are the fits of the model to experimental data. The dashed line is the calculation result for the N-doped sample without phonon scattering by bound charges. Adapted from Ref. 29.

5 January 2024 11:06:57

Boron is another common impurity of acceptor-type in diamond. Crystals containing boron with a concentration in the range from 0.5 to 5×10^{19} cm⁻³ have $\kappa(T)$ values two orders of magnitude lower at $T < 100$ K and about 5 times around 300 K than pure diamond.¹¹⁷

B. Phonon scattering by free carriers

The Ziman–Kosarev theory^{118,119} of phonon scattering on free carriers is often used to model the $\kappa(T)$ of heavily doped semiconductors in the metallic state. The interaction of phonons with free charge carriers is considered within the framework of the deformation potential approach using the effective mass approximation and the Debye spectrum for phonons. For n-type semiconductors, the rate of phonon scattering by free electrons is given by^{8,118}

$$\tau_{eZ}^{-1} = \frac{m_{\text{eff}}^2 E_d^2 k_B T}{2\pi\rho v \hbar^4} \left[x - \ln \frac{1 + \exp(Z + x/2)}{1 + \exp(Z - x/2)} \right], \quad (11)$$

where

$$Z = \frac{k_B T}{8m_{\text{eff}} v^2} x^2 + \frac{m_{\text{eff}} v^2}{2k_B T} - \frac{E_F}{k_B T}, \quad (12)$$

where E_d is the dilatation deformation potential constant, E_F is the Fermi energy, m_{eff} is the density-of-state effective mass of the carriers, ρ is the density of the crystal, v is the average phonon velocity, and $x = \hbar\omega/k_B T$, ω is the phonon frequency. Note that τ_{eZ}^{-1} does

not explicitly depend on the carrier concentration n_{ex} . In the case of a heavily doped degenerate semiconductor, Eq. (11) can be simplified to the following form:

$$\tau_{eZ}^{-1} = \frac{m_{\text{eff}}^2 E_d^2 k_B T}{2\pi\rho v \hbar^4} x. \quad (13)$$

This rate is proportional to ω (in terms of x) and, if phonon-electron scattering dominates, can lead to $\sim T^2$ dependence for $\kappa(T)$ at sufficiently low temperatures.

In the case of moderately doped semiconductors, Eq. (11) can be expressed as^{8,120,121}

$$\tau_{eZ}^{-1} = n_{\text{ex}} \frac{(2\pi m_{\text{eff}})^{1/2} E_d^2}{(k_B T)^{1/2} \rho v \hbar} \exp\left(-\frac{m_{\text{eff}} v^2}{2k_B T}\right) x. \quad (14)$$

Equation (11) is valid for phonons with wave vector $q \leq 2k_F$, where k_F is the Fermi wave vector. For phonons with $q > 2k_F$, the scattering rate is given by the following Kosarev expression:^{119,122}

$$\tau_{eK}^{-1} = n_{\text{ex}} \frac{185 m_{\text{eff}}^2 E_d^2 \psi^2}{(\rho a_B^*)^3 \hbar^3} \frac{1}{q^5}, \quad (15)$$

where ψ is the cosine of the angle between the phonon wave vector \mathbf{q} and the polarization vector \mathbf{e}_q . The scattering rate sharply decreases $\sim q^{-5}$ as the phonon wave vector increases, as a result of which scattering by free carriers becomes inefficient for phonons with large q .

$\kappa(T)$ of moderately and heavily doped semiconductors can be explained by the scattering of phonons on carriers in a mixed state, consisting of a bound (localized) and a metallic state. The number of carriers in insulating regions, where they are bound to impurities, and in metallic regions, where carriers can move freely, can be calculated using Mikoshiba's "inhomogeneity model."¹²³ This model, developed for the random distribution of impurities, assumes that the impurity which has no neighbor closer than a critical radius r_c , belongs to the insulating region. The concentration of such impurities is given by

$$n_{\text{ins}} = n \exp(-t_c), \quad t_c = (4\pi/3)n r_c^3, \quad (16)$$

where n is a total concentration of impurities. All other impurities with a concentration of n_{met} are in the metallic regions, $n_{\text{ins}} + n_{\text{met}} = n$. The critical radius can be estimated using the simplest method in the Mott transition,¹²⁴

$$r_c = (144/\pi^2)^{1/3} a_B^*. \quad (17)$$

Taking into account the scattering of phonons by bound carriers in insulating regions and by free carriers in metallic regions, the phonon $\kappa(T)$ can be calculated. Radhakrishnan and Sharma¹²² performed such calculations for Si:P with $[P] = 4.7 \times 10^{17}$ and $1.0 \times 10^{18} \text{ cm}^{-3}$ at T from 2 to 40 K and compared the results with experimental data.⁹² We noted above that the theoretical model, which takes into account only the scattering of phonons by bound electrons, approximates well the experimental data for samples

with a low P concentration ($\leq 2.5 \times 10^{17} \text{ cm}^{-3}$), but unsatisfactorily for samples with a concentration $4.7 \times 10^{17} \text{ cm}^{-3}$ (see Fig. 17). According to electrical conductivity measurements, the critical doping concentration for Si:P is $3.7 \times 10^{18} \text{ cm}^{-3}$ at 0 K.¹²⁵ Now, taking into account the additional scattering by free electrons in the framework of the Mikoshiba model, a good agreement between the calculated and measured $\kappa(T)$ for high phosphorus concentrations has been obtained. Asheghi *et al.*¹²⁶ extended such calculations to $T = 300$ K. Good agreement was also achieved for Ge doped with P-, As-, and Sb in the intermediate concentration range from 1.1×10^{17} to $5.6 \times 10^{17} \text{ cm}^{-3}$.¹⁰²

The approaches to calculating the rates of phonon scattering on charge carriers described above are constructed in the approximation of an isotropic effective mass of carriers in one valley. There are extensions of these theoretical models that take into account mass anisotropy (see, for example, the Ref. 127, and references therein) and the multi-valley nature of the conduction (valence) band.¹²⁸

Modern approaches to the thermal conductivity of solids are based on the first-principles calculations. Electron-phonon interaction as a source of phonon scattering, leading to a decrease in phonon $\kappa_{\text{ph}}(T)$, is considered in a number of recent papers in the framework of *ab initio* calculations (literature surveys are given in Refs. 129 and 130).

In most works, it is believed that a small deviation from the equilibrium of the phonon (electronic) subsystem affects the equilibrium of the electronic (phonon) subsystem, that is, the subsystems are decoupled. The interaction of phonons with electrons is considered assuming that the electrons are in an equilibrium state, and the BTE for the phonon non-equilibrium subsystem is solved in one way or another. This approach seems to be justified in the case of bound charge carriers, when the dopants do not interact with each other, but this approach is clearly flawed in the case of itinerant carriers. For heavily doped semiconductors and for metals, it is necessary to consider a single system of phonons and electrons, describing kinetic phenomena by solving the coupled BTE for the electron and phonon subsystems.

Liao *et al.*¹²¹ considered the effect of phonon-electron interaction on the $\kappa_{\text{ph}}(T)$ of Si with various charge carrier concentrations using first-principles calculations. A significant decrease in the $\kappa_{\text{ph}}(T)$ at room temperature was found with an increase in the carrier concentration above 10^{19} cm^{-3} (see Fig. 19). It should be noted that this result was obtained for a limited set of active scattering processes: phonon-phonon and phonon-electron scattering. The scattering of phonons by point defects associated with dopants and impurity isotopes was not taken into account, although the former can be quite strong for highly doped Si.

In the presence of a temperature gradient in the system of interacting charge carriers and phonons, momentum is transferred between subsystems and mutual electron-phonon drag arises: the phonon wind drags the electrons with it, but the electron flow also drags the phonon gas. In semiconductors, this drag effect creates a thermopower component, the so-called phonon drag thermopower, which is much larger in magnitude than the diffuse component due to the diffusion of electrons in a temperature gradient at low temperatures. The question arises as to how strongly this mutual drag influences the electronic and phonon thermal conductivity.

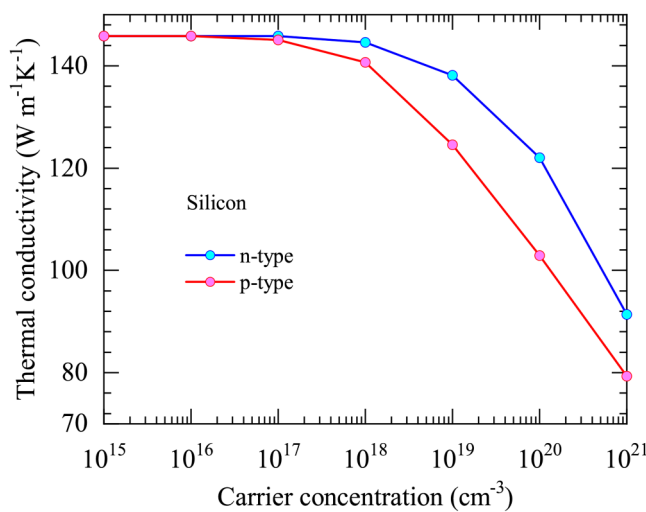


FIG. 19. Phonon thermal conductivity of Si at room temperature as a function of carrier concentration, taking into account both phonon-electron and three-phonon scattering. Adapted from Ref. 121.

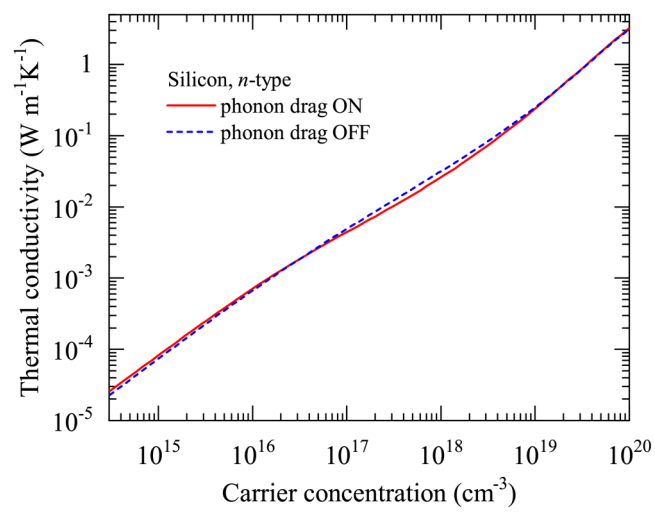


FIG. 20. Electronic thermal conductivity of *n*-type Si as a function of carrier concentration at $T = 300$ K. The red solid line is from the solution of the BTE that includes all the scattering mechanisms and the phonon drag. The blue long-dashed line is the same as the red solid line but without the phonon drag. Adapted from Ref. 132.

The most accurate answer to this question is given by solving the fully coupled BTE for electrons and phonons from first principles. Protik *et al.*¹³⁰ made similar $\kappa_{\text{ph}}(T)$ calculations for Si. For the case of very low doping (electron concentration $2.75 \times 10^{14} \text{ cm}^{-3}$), the calculated phonon thermal conductivity agrees very well with the measured conductivity of a high-purity sample with natural isotopic composition. The calculated $\kappa_{\text{ph}}(T)$ for Si with high concentration of electrons $2 \times 10^{19} \text{ cm}^{-3}$ is depressed against the one for pure silicon due to phonon scattering by electrons. This reduction of $\kappa_{\text{ph}}(T)$ is stronger at lower temperatures because the rate of phonon-phonon scattering decreases faster than that of phonon-electron scattering with temperature decrease.

Due to conservation of momentum and energy, only acoustic phonons with small wave vectors can participate in electron-phonon scattering events. The scattering rates of these “electronic” phonons determine the magnitude of phonon drag thermopower. However, “electronic” phonons make a small contribution to $\kappa_{\text{ph}}(T)$, where higher-frequency (thermal) phonons dominate. This was demonstrated by *ab initio* calculations of the contributions of phonon modes to thermopower and thermal conductivity in the case of lightly doped Si.¹³¹ As a result, the effect of electron drag on $\kappa_{\text{ph}}(T)$ is small at low temperatures.¹³⁰

With an increase in the concentration of charge carriers, it is natural to expect an increase in the electronic component $\kappa_{\text{el}}(T)$ of the thermal conductivity of the semiconductor. An approximately linear concentration dependence κ_{el} for *n*-type silicon at room temperature was obtained by Fiorentini and Bonini¹³² from first principles. The calculation results are shown in Fig. 20. Two processes of electron scattering were taken into account: electron-phonon scattering and scattering by ionized impurities; the effect of phonon drag was also taken into account. κ_{el} is much lower than $\kappa_{\text{ph}}(T)$: even at an electron concentration of $1 \times 10^{20} \text{ cm}^{-3}$, κ_{el} is only

about 2% of κ_{ph} at $T = 300$ K. As can be seen from Fig. 20, the effect of phonon drag on κ_{el} is small.

C. Magnetic field and uniaxial stress effects

Magnetic field and uniaxial stress influence the ground state of impurities in semiconductors. These fields change the energy levels and effective Bohr radius of the impurity and, therefore, affect the scattering of phonons on bound carriers. The magnitude of the effect depends on temperature, field strength, and its orientation relative to the crystal axes. The splitting Δ and the radius a_B^* are considered to be parameters through which the field influences the scattering of the bound charge.¹¹⁵

For example, in Si:B (hole concentration $9 \times 10^{16} \text{ cm}^{-3}$) at a temperature of 1.13 K, $\kappa(T)$ increases by 2 times in a magnetic field of 5 T applied in the direction $\langle 100 \rangle$.¹³³ On the contrary, in the case of *p*-type Ge lightly doped with Ga ($\leq 1.3 \times 10^{16} \text{ cm}^{-3}$) and In ($1.2 \times 10^{16} \text{ cm}^{-3}$), the field effect is generally small, $\leq 1\%$, for applied fields ≤ 7 T and $1.13 \text{ K} < T < 2.5$ K. At higher fields, up to 13 T, the effect increases but does not exceed 24%. The change in $\kappa(T)$ with a change in the field depends on the orientation of the field relative to the crystal axes and the direction of the heat flow.¹³⁴ The very weak influence of the magnetic field on $\kappa(T)$ is explained by the almost zero *g*-values of these acceptors in Ge, which leads to a very small Zeeman splitting of the ground state levels. For an undoped sample with $n_a \sim 2 \times 10^{13} \text{ cm}^{-3}$, the changes are on the limit of detection, e.g., -0.1% in 6 T at 1.6 K.

The effect of uniaxial stress on the $\kappa(T)$ of *p*-Ge lightly doped with Ga and In ($\leq 1.3 \times 10^{16} \text{ cm}^{-3}$) was studied in detail by Challis and Haseler in the temperature range of 1–4 K.¹³⁵ The compressive stress $\leq 1 \times 10^8 \text{ N m}^{-2}$ was applied along the [110] axis of the

sample in the direction of the heating flow. The uniaxial strain ϵ splits the ground state of the undistorted acceptor into two Kramers doublets separated by $\Delta = D\epsilon$, where D is the static deformation potential appropriate to the strain. The bound charge scattering should occur predominantly due to a process resonant at Δ . As the strain increases from zero, $\kappa(T)$ should first fall to a minimum value at $\Delta \sim 4k_B T$ and then rise and saturate to the value for pure Ge (recall that phonons with energy $4k_B T$ make the main contribution to the heat flux at low temperatures). The experimental results¹³⁵ are quite consistent with these theoretical expectations. For example, for a Ge:In sample with $n_a = 1.2 \times 10^{16} \text{ cm}^{-3}$, κ (1.37 K) increased more than 8 times at stress of $7 \times 10^7 \text{ N m}^{-2}$; therefore, phonon scattering by bound holes can be quenched by applying a stress.

D. Radiation damage effect

The basic radiation damage mechanisms in semiconductor materials are described, for example, in Ref. 136. We consider here the effect of displacement damage when incident radiation displaces atoms of a semiconductor from their equilibrium lattice sites. The displaced atom ends up being embedded in the lattice at another location in an interstitial site. This is called self-interstitial, and an empty site is a vacancy. The self-interstitial-vacancy pairs are called Frenkel defects. The concentration of radiation defects in a crystal depends on a number of factors, for example, the type of radiation particles, their energy, and the temperature of the crystal during irradiation. The spatial distribution of radiation defects in a sample can be nonuniform, since radiation defects can move in the lattice during irradiation and be captured by other defects, forming clusters, and aggregates. By annealing the sample at elevated temperatures, the concentration of radiation defects can be significantly reduced. Irradiation with particles can strongly reduce $\kappa(T)$ of crystals. There are few works devoted to the effect of radiation damage on $\kappa(T)$ of semiconductors. As an example, let us consider how $\kappa(T)$ of relatively pure *n*-type silicon and germanium single crystals is suppressed after irradiation with fast neutrons at fluences from 1.1×10^{17} to $3.4 \times 10^{18} \text{ n/cm}^2$ at a temperature of about 30 °C.¹³⁷

In the case of Ge, the temperature T_{\max} of maximum of $\kappa(T)$ shifts to higher temperatures after irradiations, leading to a more pronounced depression of $\kappa(T)$ below T_{\max} than at $T > T_{\max}$. In Si, however, no noticeable shift appears after irradiations, and the depressions of $\kappa(T)$ on both sides of the peak remaining comparable. The experimental data for irradiated Si can be explained by considering only the increase in the rate of scattering by point defects with the coefficient A_{pd} increasing linearly with fluence. The dominant additional scattering in the neutron-irradiated Ge appears to be scattering by bound holes. The difference between irradiation-induced scatterings in Si and Ge is attributed to the predominant effects of irradiation in these materials, silicon approaching an intrinsic behavior and germanium becoming highly *p*-type.¹³⁷ Similar results were obtained for silicon, and germanium irradiated with electrons of \sim MeV energies.

The effect of radiation damage on $\kappa(T)$ of synthetic diamonds induced by 3 MeV electrons was recently studied in detail.¹⁴⁰ As in the case of neutron-irradiated germanium considered above, radiation defects in electron-irradiated diamond with a nitrogen

impurity (about 100 ppm) create strong phonon scattering, most similar to scattering by bound charge carriers, and not to point-defect scattering. However, only elastic scattering on bound carriers, which well describes $\kappa(T)$ for unirradiated N-containing diamonds, does not give satisfactory agreement with the observed $\kappa(T)$ for irradiated diamond. Interestingly, at the same fluence, $\kappa(T)$ of irradiated pure N-free diamond is significantly lower than that of N-doped diamond at temperatures below T_m and is an order of magnitude lower at temperatures below 12 K. This is apparently due to the different charge states of defects in such diamonds. Irradiation-induced vacancies in pure diamond are in a neutral charge state, but in N-doped diamond, they are negatively charged: nitrogen donates its electron to the vacancy.¹⁴¹

VIII. BOUNDARY SCATTERING

Phonon scattering on the sample surface becomes the dominant scattering process in pure crystals at temperatures well below the conductivity peak. In this case, $\kappa(T)$ depends on the geometry of the sample: its shape, dimensions, and also on the orientation for elastically anisotropic crystals, including diamond, Si, and Ge. The character of phonon scattering on a surface (diffuse or specular) is determined by the ratio of the phonon wavelength λ and surface roughness η .

A. Specular and diffuse phonon scattering from boundaries

If $\lambda \ll \eta$, then the boundary scattering has a diffuse character and its rate is determined by the expression

$$\tau_b^{-1} = v/l_b, \quad (18)$$

where l_b is the phonon mean free path in the boundary scattering. In the case of an elastically isotropic rod, $l_b = l_C$ and $v = v_C$, where l_C is the Casimir length determined by the sample geometry, and v_C is the Casimir velocity^{142–145} given by

$$v_C = \langle s^{-2} \rangle / \langle s^{-3} \rangle, \quad (19)$$

$$\langle s^{-k} \rangle = \frac{1}{3} \sum_i s_i^{-k}, \quad k = 2, 3. \quad (20)$$

Here, s_i is the directional average phase velocity for the phonon polarization i . For a rod of the infinite length of circular cross section with diameter d , $l_C = d$, and for a rod of square cross section with side d ,

$$l_C = 1.115 d. \quad (21)$$

For the finite-length rectangular rod with length L and cross section $d_1 \times d_2$,

$$l_C = 1.115 (d_1 d_2)^{1/2} c_1 c_2, \quad (22)$$

where $c_1 < 1$ is a correction factor¹⁴⁵ depending on the ratio d_1/d_2 , and the correction factor $c_2 < 1$, which takes into account the

finite length of the rod, is equal to $1 - l_C/L$ in the first approximation.^{143,144}

In a case of elastically isotropic rod with diffusive boundary scattering, $\kappa(T)$ is given by¹⁴²

$$\kappa(T) = \frac{1}{3} C v_C l_C, \quad (23)$$

where C is the phonon volumetric heat capacity. In the boundary scattering regime, $C \sim T^3$ and, hence, $\kappa(T) \sim T^3$.

At low temperatures, when the phonon wavelength gets comparable to the surface roughness of a sample, the boundary scattering acquires the frequency dependence, and its rate can be written as¹⁴⁴

$$\tau_b^{-1} = \frac{v}{l_b} \frac{1-P}{1+P}. \quad (24)$$

Here, P is the probability of specular phonon reflection from the surface,^{146,147}

$$P = \exp[-(4\eta\omega/\pi v)^2], \quad (25)$$

where η is the root-mean-squared surface roughness.

At sufficiently low temperatures, when the wavelengths of phonons dominating in thermal conductivity (with energies $\hbar\omega \sim 4k_B T$) become much larger than η , the rate of boundary specular scattering of such phonons is proportional to ω^2 . In this case, the thermal conductivity changes as $\sim T$, and the value of $\kappa(T)$ is higher than in the case of purely diffuse boundary scattering. The theory of boundary scattering with rate presented by Eqs. (24) and (25) is often referred to as Ziman's theory.¹⁴⁶ Maznev¹⁴⁸ recently discussed the limitations of this theory.

Experimental studies by Hurst and Frankl¹⁴⁹ (see also Ref. 150) showed that the $\kappa(T)$ of well-polished samples of Si with orientation along [111] axis can be about 12 times higher than that of the samples with a rough surface at 1.5 K and approximately follows the dependence $T^{1.60}$ in the range from 1.5 to 4 K. For samples with a rough surface, the dependence $\kappa(T)$ is close to $d T^\zeta$, where $\zeta = 2.9-3.0$, and the value of d is proportional to l_C and depends on the sample orientation with respect to crystallographic axes due to the effect of phonon focusing (see Sec. VIII C). In Si, the phonon focusing effect is small for ⟨111⟩ rods.¹⁴⁵ Films of metals, nonmetals, and condensed gases less than 1 μm thick, deposited on the polished faces of Si crystals, strongly scatter phonons, which leads to a decrease in $\kappa(T)$ by approximately an order of magnitude at temperatures from 2 to 0.05 K.¹⁵⁰

A detailed investigation of the effect of various surface treatments on the low-temperature $\kappa(T)$ for Ge with different isotopic compositions including highly enriched ⁷⁰Ge(99.99%) single crystal has been performed by Asen-Palmer *et al.*³² Compared to ^{nat}Ge crystals, highly enriched crystals with very low phonon scattering rates on impurity isotopes have increased $\kappa(T)$ values, which is determined almost exclusively by phonon scattering on the sample surface over a wide temperature range on the left side of the peak. The improvement in $\kappa(T)$ for the [100] direction between the sandblasted and the most polished samples was three times.

Germanium generally exhibits qualitatively the same behavior of $\kappa(T)$ during surface polishing as Si.

In polished diamond rods and plates, the phonon mean free path l_b , found from the measured $\kappa(T)$ in the boundary scattering mode is significantly greater, 2–4 times, than the Casimir length l_C calculated based on sample geometry.^{27,29,151,152} It was proposed that the heat-carrying phonons do not reach the sample boundaries, but specular reflected within a thin subsurface damaged layer.¹⁵¹ Since the observed $\kappa(T)$ shows nearly T^3 -dependence, the rate of this specific scattering is almost independent from the phonon frequency and on temperature. Chemical etching or high-temperature annealing of the sample reduced $\kappa(T)$ in the boundary scattering regime to a value close to the theoretical expectation.^{140,151} The thickness of the damaged layer can be about 1 μm.¹⁵³ The mechanism responsible for such phonon specular reflection is still unknown.

The dependence $\kappa(T)$ for polished diamonds becomes weaker than $\sim T^3$ when the temperature drops below 10–15 K. This behavior is apparently due to frequency-dependent specular scattering of phonons at the sample boundaries [Eqs. (24) and (25)]. Fitting the theoretical model to the measured data makes it possible to estimate the effective surface roughness η : for well-polished diamond samples it is 5–10 nm,^{29,140} which is in good agreement with direct measurements of roughness R_a using an optical profilometer, which approximately corresponds to 2 times less than η .

B. Thin films and polycrystals

Equation (18) shows that the rate of boundary scattering is inversely proportional to the effective diameter of the sample and is practically independent of temperature. For samples with an effective diameter of several mm, the rate of boundary phonon scattering becomes comparable to the total rate of scattering in phonon–phonon processes and on lattice defects at low temperatures near the thermal conductivity peak (Fig. 2). As the effective diameter decreases, $\kappa(T)$ decreases at temperatures on the left side of the peak almost linearly with l_C [Eq. (23)] in the pure boundary scattering regime, but decreases relatively weakly to the right of the peak, with a maximum of thermal conductivity correspondingly decreases, and the temperature at which it occurs increases.

Phonon scattering from the sample surface can play an important role in the thermal conductivity of thin films, wires^{154,155} and polycrystals not only at low but also at high temperatures. The rate of boundary scattering is largely determined by the minimum sample size (film thickness and crystallite size) and the properties of the substrate material if the film is in contact with the substrate, or the intergranular medium in the case of some polycrystals. For example, in-plane thermal conductivity of suspended 20 nm thick silicon layer is $\sim 22 \text{ W m}^{-1} \text{ K}^{-1}$, which is nearly an order of magnitude smaller than the bulk value at room temperature.^{156,157} In the case of 1–10 μm Si films in silicon-on-insulator (SOI) wafers, calculations using Ziman's specularity parameter significantly overestimates the measured in-plane $\kappa(T)$ at temperatures from 100 to 300 K.¹⁵⁸ That is, despite the actually very smooth interface between the Si film and the amorphous SiO₂ layer, this interface behaved like a largely rough surface. This behavior can be explained by assuming that phonons with a fairly high probability transmit

TABLE III. Thermal conductivity of natural $\kappa^{(\text{nat})}$ and enriched $\kappa^{(\text{iso})}$ isotopic compositions measured for group IV semiconductors at room temperature RT, RT = 298 K. IE is the magnitude of the isotope effect at RT, IE = $100 \times (\kappa^{(\text{iso})}/\kappa^{(\text{nat})} - 1)$. $\kappa^{(\text{iso})}$ and IE correspond to crystals highly enriched in ^{12}C , ^{28}Si , and ^{70}Ge .

Crystal	$\kappa^{(\text{nat})}$ (W m ⁻¹ K ⁻¹)	$\kappa^{(\text{iso})}$ (W m ⁻¹ K ⁻¹)	IE (%)	Reference
C	2240 ± 200	3150 ± 200	41	50
Si	145 ± 3	157 ± 3	8	23
Ge	60 ± 1.2	70 ± 1.4	17	32, 64, and 74

through the interface into amorphous SiO₂, where, due to strong scattering from structural defects, their quasi-momentum becomes randomized before they return to the Si film. This behavior mimics the diffuse scattering of phonons from a rough surface. It should be noted that $\kappa(T)$ of polished bulk silicon exhibited similar behavior at low temperatures when thin films were deposited on its surface,¹⁵⁰ as discussed in Sec. VIII A.

Polycrystalline CVD diamonds exhibit peculiar $\kappa(T)$ behavior. Such diamond plates are used as a high thermal conduction material in heat spreaders and isolating windows for high power applications.^{159–161} Polycrystalline plates are characterized by a columnar grain shape, oriented along the direction of growth and perpendicular to the plane of the plates, with a typical average “diameter” of the order of several tens of micrometers. Because of the columnar grain shape, $\kappa(T)$ is anisotropic and has a higher value along the direction of the columns, reaching 2200 W m⁻¹ K⁻¹ for a column diameter of hundreds of micrometers at room temperature.^{162,163} This value is close to the thermal conductivity of the purest single crystals²⁷ (see Table III). However, the in-plane thermal conductivity $\kappa_{\text{in}}(T)$ in the direction parallel to the plates is lower, about 19.0–19.5 W m⁻¹ K⁻¹, for high-quality colorless diamond plates. Lattice defects (mostly intrinsic point defects) that accumulate near grain boundaries during CVD growth likely reduce $\kappa_{\text{in}}(T)$ of these chemically pure diamonds.^{164,165} Phonon scattering at grain boundaries and intergrain contacts negligibly reduces $\kappa_{\text{in}}(T)$ of a polycrystal (with a grain size of tens of micrometers) near and above room temperature, but this scattering significantly limits at low temperatures. Klemens¹⁶⁶ theoretically considered the scattering of phonons due to grain boundaries in polycrystalline diamond, taking into account the layer of disorder between grains. The rate of this phonon scattering varies as ω^2 at low frequencies and, therefore, decreases with decreasing temperature, in contrast to the rate of diffuse boundary scattering, which is independent of ω . As a result, $\kappa(T)$ of the polycrystal approaches the value of the single-crystal sample. This version of phonon scattering at grain boundaries well explains the measured $\kappa_{\text{in}}(T)$ of polycrystalline diamonds.^{165,167}

C. Phonon focusing effect

In an elastically isotropic medium, the phonon flux generated by a point heat source is spatially isotropic, i.e., it has the same value for any direction in the medium at a fixed distance from the source. However, in an elastically anisotropic medium, directions appear along which the energy flux due to phonons is enhanced, and along others, it is weakened compared to the isotropic case even in the case of the uniform angular distribution of phonon

wave vectors. This is how the phonon focusing effect manifests itself. This happens because the phonon phase velocity is collinear to the wave vector, and the phonon energy is transferred with the group velocity, which in general has a different direction.

The effect of phonon focusing can significantly, by tens of percent, increase the phonon mean free path compared to the Casimir length in certain directions in elastically anisotropic crystals with diffuse boundary scattering at temperatures below the conductivity peak as shown by McCurdy *et al.*¹⁴⁵ This leads to an increase in $\kappa(T)$ along the phonon focusing directions and a decrease along the defocusing directions. Cubic crystals of diamond, Si, and Ge are elastically anisotropic. For a sample in the form of a round rod, the magnitude of the increase in $\kappa(T)$ depends on the orientation [RO] of the rod and its length L . The phonon focusing effect becomes weaker for samples of finite length.¹⁶⁸ For square samples, κ also depends on the orientation of the side faces. In the case of infinitely long square cross-section rods (side size d), the theoretical phonon mean free paths $l_{[\text{RO}]}$ are presented in Table IV (see, e.g., Chap. 4 of Ref. 169). Free paths weakly depend on the orientation of the side faces, within up to a few percent. The direction of the highest $\kappa(T)$ is [100] for all group IV elemental semiconductors, but the lowest is [110] for diamond and [111] for Si and Ge. With only boundary scattering, the main contribution to $\kappa(T)$ comes from transverse phonons: for heat flow along [100], their contribution is 88% for diamond and 93% for Si and Ge.

The experimental results^{23,145} are in good agreement with theoretical calculations for Si, taking into account the finite length of the samples used.¹⁶⁸ Figure 21 presents experimental data on $\kappa(T)$ for two pairs of silicon samples oriented along [100] and [110], natural and enriched isotopic composition. On the high-temperature side of the maximum, above 31 K, the conductivity is isotropic, as it must be for cubic crystals. $\kappa_{[100]}(T)$ becomes higher than $\kappa_{[110]}(T)$ at low temperatures. The ratio $\kappa_{[100]}/\kappa_{[110]}$ for enriched ^{28}Si becomes >1.0 as the temperature drops below 31 K and remains almost constant at 1.39 at $T < 14$ K (right inset in

05 January 2024 11:09:57

TABLE IV. Phonon free paths (in units of side dimension d) in symmetric directions for rods with a square cross section and infinite length. Recall that for a rod made of an isotropic material, the free path is $1.115d$.

Crystal	$l_{[100]}$	$l_{[110]}$	$l_{[111]}$
C	1.53	1.14	1.17
Si	1.92	1.34	1.10
Ge	1.80	1.29	1.11

Fig. 21). For nat Si, the phonon focusing effect is also observed below 31 K. However, $\kappa_{[100]}/\kappa_{[110]}$ increases much more slowly with decreasing temperature due to isotope scattering, and this ratio becomes about 1.38 at 3 K. These results for 28 Si and nat Si agree with the theoretical value of 1.38 (Ref. 168) for the Si rod of finite length ($d/L = 0.1$) within experimental errors. A 3D-plot of the κ orientation dependence for a silicon rod with square cross section at 3 K is shown in Fig. 21, left inset. These data were calculated using the theoretical approach developed in Ref. 171. The Callaway-type theoretical model¹⁷⁰ well reproduces the measured data on $\kappa(T)$ for nat Si below about 10 K, but the model does not show a sharp disappearance of the phonon focusing effect above 31 K (dashed line in the right inset in Fig. 21).

Measurements on isotopically enriched crystals of 70 Ge (99.99%) gave a ratio of $\kappa_{[100]}/\kappa_{[111]} \approx 1.50$ for samples with $d/L \approx 0.05$ and noticeable misorientation, about 6° , of the sample axis from the crystallographic [100] axis (see note in Ref. 32). This measured anisotropy agrees satisfactorily with the calculated value of 1.62 for a rod of infinite length (according to data from Table IV).

Polished type-IIa natural diamond rods have identical $\kappa_{[100]}$ and $\kappa_{[110]}$ values within an experimental error of 7% at temperatures ranging from 0.5 to 20 K, as found experimentally.¹⁷² The average phonon mean free path for these samples is approximately 2.5 times the Casimir value. However, for the case of a rough surface of the rods, the “measured” ratio is $\kappa_{[100]}/\kappa_{[110]} \approx 2$, which

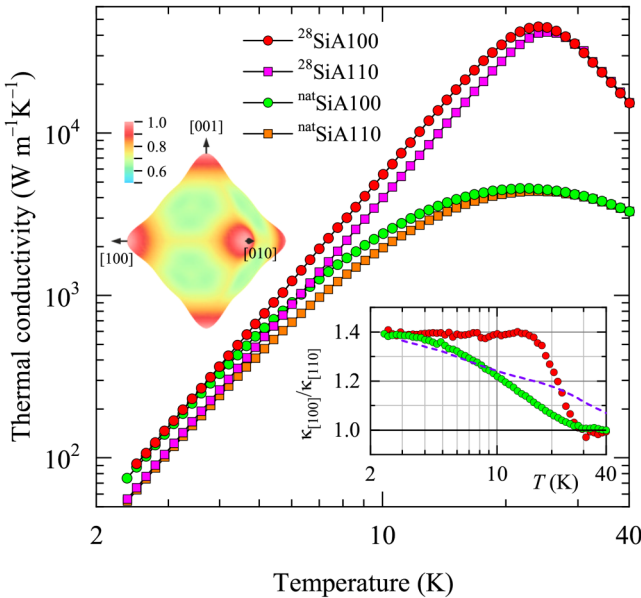


FIG. 21. Thermal conductivity for two pairs of Si samples with different orientations and isotopic compositions. The ratio of $\kappa_{[100]}/\kappa_{[110]}$ as a function of temperature is shown in the right-hand insert, and the dashed line is calculated from the data of Ref. 170. The left-hand insert shows the calculated orientation dependence of κ at 3 K, the data normalized to 1 for $\langle 100 \rangle$ direction. Adapted from Ref. 23.

significantly exceeds the theoretical prediction of 1.34. Consequently, there is only qualitative agreement between experiment and theory regarding the effect of phonon focusing in diamond.

IX. POISEUILLE FLOW OF PHONONS

Poiseuille flow (or laminar flow) in a phonon gas was first proposed by Sussman and Thellung,¹⁷³ and Gurzhi^{174,175} gave a complete description of the Poiseuille flow and thermal conductivity at low temperatures.

In an ideal isotope-free crystal, very frequent normal phonon-phonon processes, as well as very rare resistive processes, can take place. If the diameter d of the rod-shaped specimen is not very small and the following conditions are met:

$$l_N \ll d \quad \text{and} \quad l_N l_R \gg d^2, \quad (26)$$

where l_N and l_R are the mean free path for N- and R-processes in the volume of the sample, then a Poiseuille flow of phonons should be observed. Phonons are scattered through N-processes toward the walls, where momentum loss occurs. In this case, $\kappa(T)$ shows a sharp increase as T^7 -to- T^8 just before the peak value and can be represented¹⁷⁶ as

$$\kappa = \frac{1}{3} C_v v \frac{5}{32} \frac{d^2}{l_N}. \quad (27)$$

The strong T -dependence $\kappa(T)$ arises from the strong T -dependence $l_N \sim T^{-\zeta}$, $\zeta = 4-5$, and almost T^3 from C_v . Since the rate of R-processes also changes sharply with temperature, the condition equation (26) can be satisfied in a relatively narrow temperature range. Observing the Poiseuille flow provides a direct measurement of l_N . If the N-processes are not strong enough for internal reasons (weak anharmonicity of the crystal lattice), then the inequality equation (26) is not satisfied and the usual boundary scattering regime is realized with $\kappa(T) \sim T^3$ and $l_b = l_C = d$ [see Eq. (23)].

In the diffuse boundary scattering regime, the phonon flow is similar to the Knudsen flow of a rarefied gas in a cylindrical tube. The Poiseuille phonon flow increases the thermal conductivity compared to the value in the Knudsen regime. The Poiseuille flow of phonons clearly appears as a maximum in the phonon free path $l_b(T)$ at temperatures just below $\kappa(T)$ peak. The maximum value $l_b(T)$ exceeds the sample diameter d . The crossover from the Knudsen phonon flow to the Poiseuille flow occurs at temperatures when l_N is of the order of d . At these temperatures, there is a minimum $l_b(T)$, the so-called Knudsen minimum.^{177,178} Such manifestations of Poiseuille and Knudsen flow of phonon gas were discovered experimentally in almost perfect crystals of solid 4 He,^{179-181 3 He,¹⁸² and bismuth,^{183,184} which practically did not contain chemical and isotopic impurities (Bi is a monoisotopic element).}

Based on *ab initio* calculations, Ding *et al.*¹⁸⁵ recently predicted that Poiseuille flow and the Knudsen minimum can be observed in graphite even at relatively high temperatures ~ 100 K. It is noteworthy that Huang *et al.*¹⁸⁶ reported the observation of Poiseuille phonon flow in isotopically purified (0.02% 13 C) graphite

ribbons with a width of $5.5\text{ }\mu\text{m}$ up to 90 K. Hydrodynamic phonon transport, including Poiseuille flow, has been predicted in two-dimensional graphene at significantly higher temperatures and a wider temperature range than in bulk materials.¹⁸⁷ The latest achievements of phonon hydrodynamics are presented in Refs. 12, 188, and 189.

Figure 22 shows $l_b(T)$ for isotopically enriched $^{28}\text{SiA100}$ and natural $^{\text{nat}}\text{SiA100}$ crystals measured in Ref. 23. The free path was calculated using experimental data on the heat capacity of natural Si from Ref. 190 and 191 and the speed of sound $5.59 \times 10^5\text{ cm s}^{-1}$. The $l_b(T)$ curves do not demonstrate the expected anomalies inherent in the Poiseuille phonon flow. A very similar result was obtained in the case of highly enriched ^{70}Ge (99.99%).^{32,74}

X. UNSOLVED PROBLEMS

There are some important open problems in thermal conductivity of group IV semiconductors:

- Neutral and charged impurities (including vacancies) in diamond: what is the difference in the scattering efficiency, the rate of phonon scattering on defect complexes; what complexes are responsible for the dissipation of bound charge in nitrogen-doped diamonds?
- Very large phonon free path in pure polished diamonds at low temperatures, in the boundary scattering regime: what is the mechanism of interaction of phonons with lattice defects that underlies this effect; can we use this mechanism to control the mean free path of phonons; how does a layer of subsurface

damage affect the properties of a diamond detector operating at low temperatures?

- Measuring $\kappa(T)$ for isotopically pure diamond at low temperatures, including the peak region: how does isotope scattering affect $\kappa(T)$ and what is the rate of normal three-phonon scattering at these temperatures?
- Incorporating bound charge scattering and phonon focusing effects into *ab initio* $\kappa(T)$ calculations.
- Hydrodynamic effects in phonon gas in isotopically pure Si and Ge: why they are not observed.

XI. SUMMARY

The most important aspects of phonon thermal conductivity of group IV elemental semiconductors—diamond, silicon, and germanium—are described. All three crystals exhibit a temperature dependence of thermal conductivity that can be considered typical of the phonon thermal conductivity of almost ideal crystals.

The same cubic symmetry of the crystal lattice greatly simplifies the theoretical consideration of the thermal conductivity of these crystals. Their intrinsic thermal conductivity is determined by the dynamics of the crystal lattice: phonon dispersion and phonon–phonon interaction. Si and Ge, due to the close values of interatomic force bonds, have similar lattice constants and very similar dispersion dependencies of phonons, their difference is primarily due to different atomic masses of these elements. Due to these circumstances, $\kappa(T)$ of Si and Ge correlates inversely with atomic mass. Diamond does not fit into this picture because of the very strong interatomic bonds. Diamond exhibits highest $\kappa(T)$ among bulk materials. A significant role in its thermal conductivity even at ambient temperature is played by normal phonon–phonon scattering. This is the reason for the high sensitivity of the $\kappa(T)$ of diamond to defects in the crystal lattice, including impurity isotopes. Even such a low content of the ^{13}C isotope in a natural mixture of carbon isotopes, such as about 1%, reduces the $\kappa(T)$ of diamond by almost 50% at room temperature.

In the semiconductors under consideration at room temperature, optical phonons make an order of magnitude smaller contribution to the heat flux than acoustic ones. However, phonon–phonon processes involving optical phonons significantly limit, by tens of percent, the heat flow due to acoustic phonons.

Three-phonon scattering is the dominant intrinsic scattering that determines $\kappa(T)$ of group IV semiconductors, and four-phonon scattering is negligible at moderate and low temperatures, $<0.4 T_D$, but at high temperatures, the latter can significantly suppress thermal conductivity by about 30% at 1000 K. Renormalization of phonons due to weak anharmonicity of interatomic bonds leads to a weak effect on the calculated value of $\kappa(T)$ at moderate and negligible at low temperatures.

Electronic thermal conductivity increases with temperature, but becomes significant compared to phonon conductivity in pure Si and Ge only at temperatures above $1.6 T_D$ with the dominance of the bipolar term.

Scattering of phonons on non-interacting point defects occurs due to the mass and bond perturbations that they introduce into the crystal lattice, as well as due to the deformation fields around

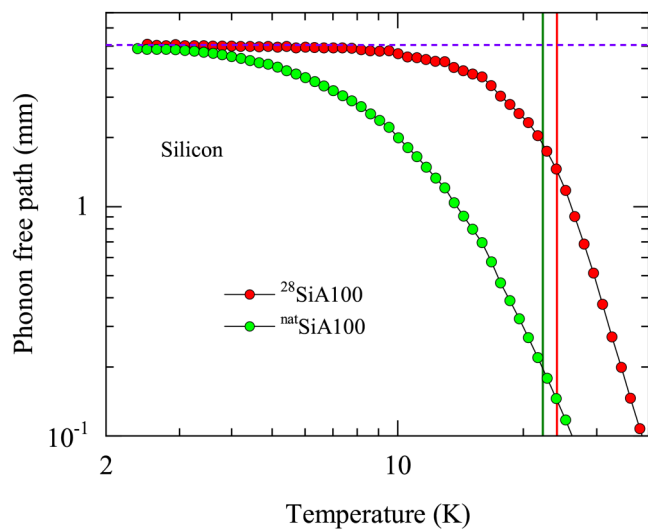


FIG. 22. Phonon mean free path as a function of temperature for Si single crystals $^{28}\text{SiA100}$ and $^{\text{nat}}\text{SiA100}$. The experimental data for $\kappa(T)$ were taken Ref. 23. The dashed line is the limit value $l(T \rightarrow 0)$. The red and green lines indicate the temperature values T_{\max} at which $\kappa(T)$ reaches a maximum for $^{28}\text{SiA100}$ and $^{\text{nat}}\text{SiA100}$, respectively.

the impurity atoms. If the mass difference between the impurity and host atoms is small, then scattering due to bond perturbations predominates, otherwise mass perturbations make a large contribution to phonon scattering; the lattice strain effect plays a minor role in reducing thermal conductivity at ambient temperature. Single vacancies are very effective scatterers of phonons in diamond.

Electroactive impurities in these semiconductors reduce $\kappa(T)$, with the effect being most pronounced at low temperatures. In lightly doped materials, phonons are scattered by neutral impurities due to the interaction of phonons with charge carriers bound to the impurities. This scattering can dominate conductivity on the low temperature side of the maximum. At a high concentration of impurities, when they form an impurity band of charge carriers, the interaction of phonons with free charge carriers can significantly reduce the phonon thermal conductivity at room temperature and above. Electronic thermal conductivity under these conditions is significantly less than phonon conductivity.

Radiation damage to crystals due to irradiation with high-energy particles (electrons or neutrons) strongly suppresses thermal conductivity (by orders of magnitude) at fluences above 10^{17} cm^{-2} . The suppression is strongest at low temperatures, when point defect scattering is ineffective, suggesting that electrically active radiation defects are responsible for the suppression of $\kappa(T)$.

At very low temperatures, when phonons are scattered not in the bulk of the sample, but only on its surface, $\kappa(T)$ is very sensitive to the state of the sample surface in the case of a polished sample. Unlike Si and Ge, polished diamond exhibits frequency-independent specular scattering of phonons. The mechanism of interaction of phonons with the surface or with defects in the near-surface damage layer is unknown.

Due to phonon focusing, thermal conductivity becomes anisotropic for cubic crystals of group IV semiconductors with the highest $\kappa(T)$ along the [100] axis. The effect can reach 50% or more.

Hydrodynamic effects in the $\kappa(T)$ of isotopically and chemically pure Si and Ge crystals have not been detected.

ACKNOWLEDGMENTS

A.V.I. acknowledges support from the Russian Science Foundation (Grant No. 23-29-00214). David Broido, Lucas Lindsay, and Navaneetha Krishnan Ravichandran provided the data used to make Figs. 6 and 8; Teng Fang and Tiejun Zhu provided the data used to make Fig. 11. The author thanks A. M. Gibin, I. G. Kuleyev, V. G. Ralchenko, and A. N. Taldenkov for useful and enlightening discussions.

AUTHOR DECLARATIONS

Conflict of Interest

The authors have no conflicts to disclose.

Author Contributions

A. V. Inyushkin: Writing – original draft (equal); Writing – review & editing (equal).

DATA AVAILABILITY

Data sharing is not applicable to this article as no new data were created or analyzed in this study.

REFERENCES

- ¹S. Chen, Q. Wu, C. Mishra, J. Kang, H. Zhang, K. Cho, W. Cai, A. A. Balandin, and R. S. Ruoff, "Thermal conductivity of isotopically modified graphene," *Nat. Mater.* **11**, 203–207 (2012).
- ²R. Berman, *Thermal Conduction in Solids*, Oxford Studies in Physics (Clarendon Press, Oxford, 1976).
- ³P. G. Klemens, "Thermal conductivity and lattice vibrational modes," in *Solid State Physics*, edited by F. Seitz and D. Turnbull (Academic Press, New York, 1958), Vol. 7, pp. 1–98.
- ⁴J. Callaway, "Model for lattice thermal conductivity at low temperatures," *Phys. Rev.* **113**, 1046–1051 (1959).
- ⁵J. Ziman, *Electrons and Phonons: The Theory of Transport Phenomena in Solids*, International Series of Monographs on Physics (Oxford University Press, Oxford, 2001).
- ⁶P. Carruthers, "Theory of thermal conductivity of solids at low temperatures," *Rev. Mod. Phys.* **33**, 92–138 (1961).
- ⁷G. P. Srivastava, "Lattice thermal conduction mechanism in solids," in *High Thermal Conductivity Materials*, edited by S. L. Shindé and J. S. Goela (Springer, New York, 2006), Chap. 1, pp. 1–35.
- ⁸G. P. Srivastava, "Theories of phonon transport in bulk and nanostructured solids," in *Length-Scale Dependent Phonon Interactions*, edited by S. L. Shindé and G. P. Srivastava (Springer, New York, 2014), Chap. 3, pp. 81–114.
- ⁹D. T. Morelli and G. A. Slack, "High lattice thermal conductivity solids," in *High Thermal Conductivity Materials*, edited by S. L. Shindé and J. S. Goela (Springer, New York, 2006), Chap. 2, pp. 37–68.
- ¹⁰J. Garg, N. Bonini, and N. Marzari, "First-principles determination of phonon lifetimes, mean free paths, and thermal conductivities in crystalline materials: Pure silicon and germanium," in *Length-Scale Dependent Phonon Interactions*, edited by S. L. Shindé and G. P. Srivastava (Springer, New York, 2014), Chap. 4, pp. 115–136.
- ¹¹N. Mingo, D. A. Stewart, D. A. Broido, L. Lindsay, and W. Li, "Ab initio thermal transport," in *Length-Scale Dependent Phonon Interactions*, edited by S. L. Shindé and G. P. Srivastava (Springer, New York, 2014), Chap. 5, pp. 137–173.
- ¹²L. Lindsay, C. Hua, X. L. Ruan, and S. Lee, "Survey of ab initio phonon thermal transport," *Mater. Today Phys.* **7**, 106–120 (2018).
- ¹³A. J. H. McGaughey, A. Jain, H.-Y. Kim, and B. Fu, "Phonon properties and thermal conductivity from first principles, lattice dynamics, and the Boltzmann transport equation," *J. Appl. Phys.* **125**, 011101 (2019).
- ¹⁴L. Lindsay, A. Katre, A. Cepellotti, and N. Mingo, "Perspective on ab initio phonon thermal transport," *J. Appl. Phys.* **126**, 050902 (2019).
- ¹⁵X. Qian, J. Zhou, and G. Chen, "Phonon-engineered extreme thermal conductivity materials," *Nat. Mater.* **20**, 1188–1202 (2021).
- ¹⁶R. Peierls, "Zur kinetischen theorie der wärmeleitung in kristallen," *Ann. Phys.* **395**, 1055–1101 (1929).
- ¹⁷N. K. Ravichandran and D. Broido, "Unified first-principles theory of thermal properties of insulators," *Phys. Rev. B* **98**, 085205 (2018).
- ¹⁸J. Nye, *Physical Properties of Crystals: Their Representation by Tensors and Matrices*, Oxford Science Publications (Clarendon Press, New York, 1985).
- ¹⁹*Thermal Conductivity*, edited by R. P. Tye (Academic Press, London, 1969), Chaps. 3–6, Vol. 1.
- ²⁰T. M. Tritt and D. Weston, "Measurement techniques and considerations for determining thermal conductivity of bulk materials," in *Thermal Conductivity: Theory, Properties, and Applications*, edited by T. M. Tritt (Springer US, Boston, MA, 2004), pp. 187–203.
- ²¹T. Borca-Tasciuc and G. Chen, "Experimental techniques for thin-film thermal conductivity characterization," in *Thermal Conductivity: Theory*,

- Properties, and Applications*, edited by T. M. Tritt (Springer US, Boston, MA, 2004), pp. 205–237.
- ²²R. Berman, “Thermal conductivity measurements,” in *Experimental Cryophysics*, edited by F. E. Hoare, L. C. Jackson, and N. Kurti (Butterworths, London, 1961), Chap. 10.10, pp. 327–336.
- ²³A. V. Inyushkin, A. N. Taldenkov, J. W. Ager, E. E. Haller, H. Riemann, N. V. Abrosimov, H.-J. Pohl, and P. Becker, “Ultrahigh thermal conductivity of isotopically enriched silicon,” *J. Appl. Phys.* **123**, 095112 (2018).
- ²⁴E. T. Swartz and R. O. Pohl, “Thermal boundary resistance,” *Rev. Mod. Phys.* **61**, 605–668 (1989).
- ²⁵J. W. Ekin, *Experimental Techniques for Low-Temperature Measurements. Cryostat Design, Material Properties, and Superconductor Critical-Current Testing* (Oxford University Press, New York, 2006).
- ²⁶G. K. White, *Experimental Techniques in Low-Temperature Physics*, 3rd ed. (Clarendon, Oxford University Press, Oxford, 1979).
- ²⁷A. V. Inyushkin, A. N. Taldenkov, V. G. Ralchenko, A. P. Bolshakov, A. V. Koliadin, and A. N. Katrusha, “Thermal conductivity of high purity synthetic single crystal diamonds,” *Phys. Rev. B* **97**, 144305 (2018).
- ²⁸V. G. Ralchenko, A. V. Inyushkin, G. Shu, B. Dai, I. A. Karateev, A. P. Bolshakov, A. A. Khomich, E. E. Ashkinazi, E. Zavedeev, J. Han, and J. Zhu, “Thermal conductivity of diamond mosaic crystals grown by chemical vapor deposition: Thermal resistance of junctions,” *Phys. Rev. Appl.* **16**, 014049 (2021).
- ²⁹A. V. Inyushkin, A. N. Taldenkov, V. G. Ralchenko, G. Shu, B. Dai, A. P. Bolshakov, A. A. Khomich, E. E. Ashkinazi, K. N. Boldyrev, A. V. Khomich, J. Han, V. I. Konov, and J. Zhu, “Thermal conductivity of pink CVD diamond: Influence of nitrogen-related centers,” *J. Appl. Phys.* **133**, 025102 (2023).
- ³⁰C. J. Glassbrenner and G. A. Slack, “Thermal conductivity of silicon and germanium from 3 K to the melting point,” *Phys. Rev.* **134**, A1058–A1069 (1964).
- ³¹J. R. Olson, R. O. Pohl, J. W. Vandersande, A. Zoltan, T. R. Anthony, and W. F. Banholzer, “Thermal conductivity of diamond between 170 and 1200 K and the isotope effect,” *Phys. Rev. B* **47**, 14850–14856 (1993).
- ³²M. Asen-Palmer, K. Bartkowski, E. Gmelin, M. Cardona, A. P. Zhernov, A. V. Inyushkin, A. N. Taldenkov, V. I. Ozhogin, K. M. Itoh, and E. E. Haller, “Thermal conductivity of germanium crystals with different isotopic compositions,” *Phys. Rev. B* **56**, 9431–9447 (1997).
- ³³C. Y. Ho, R. W. Powell, and P. E. Liley, “Thermal conductivity of the elements,” *J. Phys. Chem. Ref. Data* **1**, 279–421 (1972).
- ³⁴R. A. Guyer and J. A. Krumhansl, “Solution of the linearized phonon Boltzmann equation,” *Phys. Rev.* **148**, 766–778 (1966).
- ³⁵G. Leibfried and E. Schlömann, “Warmleitund in elektrische isolierenden kristallen,” Nachr. Akad. Wiss. Göttingen, Math.-Phys. Kl. IIa, 71–93 (1954).
- ³⁶G. A. Slack, “Nonmetallic crystals with high thermal conductivity,” *J. Phys. Chem. Solids* **34**, 321–335 (1973).
- ³⁷A. Konti and Y. P. Varshni, “Debye temperatures of 24 cubic elements by three methods,” *Can. J. Phys.* **47**, 2021–2029 (1969).
- ³⁸A. Konti and Y. P. Varshni, “Debye temperatures of alkali halides,” *Can. J. Phys.* **49**, 3115–3121 (1971).
- ³⁹A. G. Every, “General closed-form expressions for acoustic waves in elastically anisotropic solids,” *Phys. Rev. B* **22**, 1746–1760 (1980).
- ⁴⁰H. Xie, J. Yan, X. Gu, and H. Bao, “A scattering rate model for accelerated evaluation of lattice thermal conductivity bypassing anharmonic force constants,” *J. Appl. Phys.* **125**, 205104 (2019).
- ⁴¹S. A. Miller, P. Gorai, B. R. Ortiz, A. Goyal, D. Gao, S. A. Barnett, T. O. Mason, G. J. Snyder, Q. Lv, V. Stevanović, and E. S. Toberer, “Capturing anharmonicity in a lattice thermal conductivity model for high-throughput predictions,” *Chem. Mater.* **29**, 2494–2501 (2017).
- ⁴²D. A. Broido, L. Lindsay, and A. Ward, “Thermal conductivity of diamond under extreme pressure: A first-principles study,” *Phys. Rev. B* **86**, 115203 (2012).
- ⁴³S. Baroni, S. de Gironcoli, A. D. Corso, and P. Giannozzi, “Phonons and related crystal properties from density-functional perturbation theory,” *Rev. Mod. Phys.* **73**, 515–562 (2001).
- ⁴⁴M. Omini and A. Sparavigna, “Beyond the isotropic-model approximation in the theory of thermal conductivity,” *Phys. Rev. B* **53**, 9064–9073 (1996).
- ⁴⁵D. A. Broido, M. Malorny, G. Birner, N. Mingo, and D. A. Stewart, “Intrinsic lattice thermal conductivity of semiconductors from first principles,” *Appl. Phys. Lett.* **91**, 231922 (2007).
- ⁴⁶L. Lindsay, D. A. Broido, and T. L. Reinecke, “*Ab initio* thermal transport in compound semiconductors,” *Phys. Rev. B* **87**, 165201 (2013).
- ⁴⁷L. Lindsay and D. A. Broido, “Three-phonon phase space and lattice thermal conductivity in semiconductors,” *J. Phys.: Condens. Matter* **20**, 165209 (2008).
- ⁴⁸M. Omini and A. Sparavigna, “Heat transport in dielectric solids with diamond structure,” *Nuovo Cimento D* **19**, 1537–1563 (1997).
- ⁴⁹D. G. Onn, A. Witke, Y. Z. Qiu, T. R. Anthony, and W. F. Banholzer, “Some aspects of the thermal conductivity of isotopically enriched diamond single crystals,” *Phys. Rev. Lett.* **68**, 2806–2809 (1992).
- ⁵⁰L. Wei, P. K. Kuo, R. L. Thomas, T. R. Anthony, and W. F. Banholzer, “Thermal conductivity of isotopically modified single crystal diamond,” *Phys. Rev. Lett.* **70**, 3764–3767 (1993).
- ⁵¹A. Ward, D. A. Broido, D. A. Stewart, and G. Deinzer, “*Ab initio* theory of the lattice thermal conductivity in diamond,” *Phys. Rev. B* **80**, 125203 (2009).
- ⁵²L. Lindsay, D. A. Broido, and T. L. Reinecke, “First-principles determination of ultrahigh thermal conductivity of boron arsenide: A competitor for diamond?,” *Phys. Rev. Lett.* **111**, 025901 (2013).
- ⁵³Z. Tian, K. Esfarjani, J. Shiomi, A. S. Henry, and G. Chen, “On the importance of optical phonons to thermal conductivity in nanostructures,” *Appl. Phys. Lett.* **99**, 053122 (2011).
- ⁵⁴S. Mukhopadhyay, L. Lindsay, and D. J. Singh, “Optic phonons and anisotropic thermal conductivity in hexagonal Ge₂Sb₂Te₅,” *Sci. Rep.* **6**, 37076 (2016).
- ⁵⁵T. Feng, L. Lindsay, and X. Ruan, “Four-phonon scattering significantly reduces intrinsic thermal conductivity of solids,” *Phys. Rev. B* **96**, 161201 (2017).
- ⁵⁶T. Feng and X. Ruan, “Higher-order phonon scattering: advancing the quantum theory of phonon linewidth, thermal conductivity and thermal radiative properties,” in *Nanoscale Energy Transport*, 2053–2563 (IOP Publishing, 2020), pp. 2–1 to 2–44.
- ⁵⁷C. Y. Ho, R. W. Powell, and P. E. Liley, “Thermal conductivity of the elements: A comprehensive review,” *J. Phys. Chem. Ref. Data* **3**, I–1–I–796 (1974).
- ⁵⁸T. Feng and X. Ruan, “Quantum mechanical prediction of four-phonon scattering rates and reduced thermal conductivity of solids,” *Phys. Rev. B* **93**, 045202 (2016).
- ⁵⁹Y. Xia, “Revisiting lattice thermal transport in PbTe: The crucial role of quartic anharmonicity,” *Appl. Phys. Lett.* **113**, 073901 (2018).
- ⁶⁰X. Gu, S. Li, and H. Bao, “Thermal conductivity of silicon at elevated temperature: Role of four-phonon scattering and electronic heat conduction,” *Int. J. Heat Mass Transf.* **160**, 120165 (2020).
- ⁶¹G. A. Slack and C. Glassbrenner, “Thermal conductivity of germanium from 3 K to 1020 K,” *Phys. Rev.* **120**, 782–789 (1960).
- ⁶²G. Guo, X. Yang, J. Carrete, and W. Li, “Revisiting the thermal conductivity of Si, Ge and diamond from first principles: Roles of atomic mass and interatomic potential,” *J. Phys.: Condens. Matter* **33**, 285702 (2021).
- ⁶³A. V. Inyushkin, A. N. Taldenkov, A. V. Gusev, A. M. Gibin, V. A. Gavva, and E. A. Kozyrev, “Thermal conductivity of the single-crystal monoisotopic ²⁹Si in the temperature range 2.4–410 K,” *Phys. Solid State* **55**, 235–239 (2013).
- ⁶⁴A. M. Gibin, N. V. Abrosimov, A. D. Bulanov, and V. A. Gavva, “Thermal conductivity of single crystals of isotopically enriched germanium ⁷⁰Ge, ⁷²Ge, ⁷⁴Ge in the range 80–310 K,” *Phys. Solid State* **55**, 1448–1452 (2023).
- ⁶⁵I. Pomeranchuk, “Thermal conductivity of dielectrics at temperatures lower than that of Debye,” *J. Phys. USSR* **6**, 237 (1942).
- ⁶⁶T. H. Geballe and G. W. Hull, “Isotopic and other types of thermal resistance in germanium,” *Phys. Rev.* **110**, 773–775 (1958).
- ⁶⁷P. G. Klemens and A. A. Maradudin, “Lattice distortion due to isotopes in solid helium,” *Phys. Rev.* **123**, 804–806 (1961).
- ⁶⁸H. D. Jones, “Theory of the isotopic impurity in solid helium and neon,” *Phys. Rev. A* **1**, 71–85 (1970).
- ⁶⁹Y. Kagan and A. P. Zhernov, “Electrical conductivity of isotopically disordered metals,” *Sov. Phys. JETP* **26**, 999–1002 (1968).

- ⁷⁰A. P. Zhernov, "Static displacements of atoms near isotopic impurities and residual resistivity," *J. Exp. Theor. Phys.* **87**, 1172–1178 (1998).
- ⁷¹A. P. Zhernov and A. V. Inyushkin, "Effect of isotopic composition on phonon modes. Static atomic displacements in crystals," *Phys. Usp.* **44**, 785–811 (2001).
- ⁷²S. Tamura, "Isotope scattering of dispersive phonons in Ge," *Phys. Rev. B* **27**, 858–866 (1983).
- ⁷³A. A. Kaminskii, V. G. Ralchenko, H. Yoneda, A. P. Bolshakov, and A. V. Inyushkin, "Stimulated Raman scattering-active isotopically pure ¹²C and ¹³C diamond crystals: A milestone in the development of diamond photonics," *JETP Lett.* **104**, 347–352 (2016).
- ⁷⁴V. I. Ozhogin, A. V. Inyushkin, A. N. Taldenkov, A. V. Tikhomirov, G. E. Popov, E. Haller, and K. Itoh, "Isotope effect in the thermal conductivity of germanium single crystals," *JETP Lett.* **63**, 490–494 (1996).
- ⁷⁵A. Sparavigna, "Influence of isotope scattering on the thermal conductivity of diamond," *Phys. Rev. B* **65**, 064305 (2002).
- ⁷⁶G. Fugallo, M. Lazzeri, L. Paulatto, and F. Mauri, "Ab initio variational approach for evaluating lattice thermal conductivity," *Phys. Rev. B* **88**, 045430 (2013).
- ⁷⁷P. G. Klemens, "The scattering of low-frequency lattice waves by static imperfections," *Proc. Phys. Soc. A* **68**, 1113–1128 (1955).
- ⁷⁸L. A. Turk and P. G. Klemens, "Phonon scattering by impurity platelet precipitates in diamond," *Phys. Rev. B* **9**, 4422–4428 (1974).
- ⁷⁹N. Mingo, K. Esfarjani, D. A. Broido, and D. A. Stewart, "Cluster scattering effects on phonon conduction in graphene," *Phys. Rev. B* **81**, 045408 (2010).
- ⁸⁰E. N. Economou, *Green's Functions in Quantum Physics*, Springer Series in Solid-State Sciences (Springer, 2006).
- ⁸¹A. Kundu, N. Mingo, D. A. Broido, and D. A. Stewart, "Role of light and heavy embedded nanoparticles on the thermal conductivity of SiGe alloys," *Phys. Rev. B* **84**, 125426 (2011).
- ⁸²Y. Lee, S. Lee, and G. S. Hwang, "Effects of vacancy defects on thermal conductivity in crystalline silicon: A nonequilibrium molecular dynamics study," *Phys. Rev. B* **83**, 125202 (2011).
- ⁸³Y. Lee and G. S. Hwang, "Mechanism of thermal conductivity suppression in doped silicon studied with nonequilibrium molecular dynamics," *Phys. Rev. B* **86**, 075202 (2012).
- ⁸⁴T. Murakami, T. Shiga, T. Hori, K. Esfarjani, and J. Shiomi, "Importance of local force fields on lattice thermal conductivity reduction in PbTe_{1-x}Se_x alloys," *Europhys. Lett.* **102**, 46002 (2013).
- ⁸⁵H. B. Dyer, F. A. Raal, L. D. Preez, and J. H. N. Loubser, "Optical absorption feature associated with paramagnetic nitrogen in diamond," *Philos. Mag. A: J. Theor. Exp. Appl. Phys.* **11**, 763–774 (1965).
- ⁸⁶R. Berman, P. R. W. Hudson, and M. Martinez, "Nitrogen in diamond: Evidence from thermal conductivity," *J. Phys. C* **8**, L430–L434 (1975).
- ⁸⁷G. A. Slack, "Thermal conductivity of pure and impure silicon, silicon carbide, and diamond," *J. Appl. Phys.* **35**, 3460–3466 (1964).
- ⁸⁸J. W. Vandersande, "A correlation between the infrared absorption features and the low temperature thermal conductivity of different types of natural diamonds," *J. Phys. C* **13**, 757–764 (1980).
- ⁸⁹J. P. Goss, R. J. Eyre, and P. R. Briddon, "Theoretical models for doping diamond for semiconductor applications," *Phys. Status Solidi B* **245**, 1679–1700 (2008).
- ⁹⁰N. A. Katcho, J. Carrete, W. Li, and N. Mingo, "Effect of nitrogen and vacancy defects on the thermal conductivity of diamond: An ab initio Green's function approach," *Phys. Rev. B* **90**, 094117 (2014).
- ⁹¹M. Fava, N. H. Protik, C. Li, N. K. Ravichandran, J. Carrete, A. van Roekeghem, G. K. H. Madsen, N. Mingo, and D. Broido, "How dopants limit the ultrahigh thermal conductivity of boron arsenide: A first principles study," *npj Comput. Mater.* **7**, 54 (2021).
- ⁹²D. Fortier and K. Suzuki, "Effect of P donors on thermal phonon scattering in Si," *J. Phys. (Paris)* **37**, 143–147 (1976).
- ⁹³T. Fang, J. Xin, C. Fu, D. Li, X. Zhao, C. Felser, and T. Zhu, "Influence of electron-phonon interaction on the lattice thermal conductivity in single-crystal Si," *Ann. Phys. (Berl.)* **532**, 1900435 (2020).
- ⁹⁴A. M. de Goér, M. Locatelli, and K. Lassmann, "A study of the ground state of acceptors in silicon from thermal transport experiments," *J. Phys. (Paris) Colloq.* **42**, C6–235–C6–237 (1981).
- ⁹⁵M. G. Holland and L. J. Neuringer, "The effect of impurities on the lattice thermal conductivity of silicon," in *Proceedings of the International Conference on the Physics of Semiconductors* (Institute of Physics and the Physical Society, London, 1962), pp. 474–481.
- ⁹⁶T. Sota, K. Suzuki, and D. Fortier, "Low-temperature thermal conductivity of heavily doped p-type semiconductors," *J. Phys. C* **17**, 5935–5944 (1984).
- ⁹⁷J. A. Carruthers, T. H. Geballe, H. M. Rosenberg, J. M. Ziman, and K. A. G. Mendelsohn, "The thermal conductivity of germanium and silicon between 2 and 300 K," *Proc. R. Soc. Lond. Ser. A* **238**, 502–514 (1957).
- ⁹⁸S. R. Bakhchieva, N. P. Kekelidze, and M. G. Kekua, "Thermal conductivity of germanium doped with silicon, tin, and aluminium," *Phys. Status Solidi A* **83**, 139–145 (1984).
- ⁹⁹J. F. Goff and N. Pearlman, "Thermal transport properties of n-type Ge at low temperatures," *Phys. Rev.* **140**, A2151–A2169 (1965).
- ¹⁰⁰M. P. Mathur and N. Pearlman, "Phonon scattering by neutral donors in germanium," *Phys. Rev.* **180**, 833–845 (1969).
- ¹⁰¹H. J. Albany and G. Laurence, "Donor concentration dependence of electron-phonon scattering in antimony-doped germanium," *Solid State Commun.* **7**, 63–66 (1969).
- ¹⁰²V. Radhakrishnan and P. C. Sharma, "Electron-phonon interaction in P-, As-, and Sb-doped germanium in the intermediate concentration region," *Can. J. Phys.* **58**, 1268–1274 (1980).
- ¹⁰³R. W. Keyes, "Low-temperature thermal resistance of n-type germanium," *Phys. Rev.* **122**, 1171–1176 (1961).
- ¹⁰⁴J. M. Luttinger and W. Kohn, "Motion of electrons and holes in perturbed periodic fields," *Phys. Rev.* **97**, 869–883 (1955).
- ¹⁰⁵W. Kohn, *Shallow Impurity States in Silicon and Germanium* (Academic Press, 1957), pp. 257–320.
- ¹⁰⁶A. K. Ramdas and S. Rodriguez, "Spectroscopy of the solid-state analogues of the hydrogen atom: Donors and acceptors in semiconductors," *Rep. Prog. Phys.* **44**, 1297–1387 (1981).
- ¹⁰⁷B. L. Bird and N. Pearlman, "Thermal conductivity of n-type germanium from 0.3 to 4.2 K," *Phys. Rev. B* **4**, 4406–4416 (1971).
- ¹⁰⁸P. C. Kwok, "Acoustic attenuation by neutral donor impurity atoms in germanium," *Phys. Rev.* **149**, 666–674 (1966).
- ¹⁰⁹L. J. Challis, A. M. de Goér, and S. C. Haseler, "Thermal conductivity of p-Ge down to 50 mK," *Phys. Rev. Lett.* **39**, 558–561 (1977).
- ¹¹⁰A. Adolf, D. Fortier, J. H. Albany, and K. Suzuki, "Effect of internal strains on thermal-phonon scattering in Li-doped Si," *Phys. Rev. B* **21**, 5651–5655 (1980).
- ¹¹¹J. F. Goff and N. Pearlman, "Erratum: Thermal transport properties of n-type Ge at low temperatures," *Phys. Rev.* **149**, 734(E) (1966).
- ¹¹²M. N. Alexander and D. F. Holcomb, "Semiconductor-to-metal transition in n-type group IV semiconductors," *Rev. Mod. Phys.* **40**, 815–829 (1968).
- ¹¹³P. P. Edwards and M. J. Sienko, "Universality aspects of the metal-nonmetal transition in condensed media," *Phys. Rev. B* **17**, 2575–2581 (1978).
- ¹¹⁴K. Suzuki and N. Mikoshiba, "On the low-temperature thermal conductivity of n-Ge," *J. Phys. Soc. Jpn.* **31**, 186–189 (1971).
- ¹¹⁵K. Suzuki and N. Mikoshiba, "Effects of uniaxial stress and magnetic field on the low-temperature thermal conductivity of p-type Ge and Si," *J. Phys. Soc. Jpn.* **31**, 44–53 (1971); , "Erratum: Effects of uniaxial stress and magnetic field on the low-temperature thermal conductivity of p-type Ge and Si," *J. Phys. Soc. Jpn.* **32**, 586(E) (1972).
- ¹¹⁶K. Suzuki and N. Mikoshiba, "Low-temperature thermal conductivity of p-type Ge and Si," *Phys. Rev. B* **3**, 2550–2556 (1971).
- ¹¹⁷D. Prikhodko, S. Tarelkin, V. Bormashov, A. Golovanov, M. Kuznetsov, D. Teteruk, N. Kornilov, A. Volkov, and A. Buga, "Low temperature thermal conductivity of heavily boron-doped synthetic diamond: Influence of boron-related structure defects," *J. Superhard Mater.* **41**, 24–31 (2019).
- ¹¹⁸J. M. Ziman, "XVII. The effect of free electrons on lattice conduction," *Philos. Mag. A: J. Theor. Exp. Appl. Phys.* **1**, 191–198 (1956).

- ¹¹⁹V. V. Kosarev, "Scattering of phonons by carriers in the field of charged impurities," Sov. Phys. JETP **33**, 793–795 (1971).
- ¹²⁰J. E. Parrott, "Heat conduction mechanisms in semiconducting materials," Rev. Int. Hautes Temp. Refract. **16**, 393–403 (1979).
- ¹²¹B. Liao, B. Qiu, J. Zhou, S. Huberman, K. Esfarjani, and G. Chen, "Significant reduction of lattice thermal conductivity by the electron-phonon interaction in silicon with high carrier concentrations: A first-principles study," Phys. Rev. Lett. **114**, 115901 (2015).
- ¹²²V. Radhakrishnan, P. C. Sharma, and M. Singh, "Electron-phonon interaction in P-doped silicon at low temperatures," Z. Phys. B: Condens. Matter **39**, 15–19 (1980).
- ¹²³N. Mikoshiba, "Model for the metal-nonmetal transition in impure semiconductors," Rev. Mod. Phys. **40**, 833–838 (1968).
- ¹²⁴N. F. Mott, "The transition to the metallic state," Philos. Mag. A: J. Theor. Exp. Appl. Phys. **6**, 287–309 (1961).
- ¹²⁵T. F. Rosenbaum, K. Andres, G. A. Thomas, and R. N. Bhatt, "Sharp metal-insulator transition in a random solid," Phys. Rev. Lett. **45**, 1723–1726 (1980).
- ¹²⁶M. Asheghi, K. Kurabayashi, R. Kasnavi, and K. E. Goodson, "Thermal conduction in doped single-crystal silicon films," J. Appl. Phys. **91**, 5079–5088 (2002).
- ¹²⁷M. K. Roy and B. K. Deb, "Phonon conductivity in As-, Sb-, and P-doped Ge for intermediate donor concentration," Phys. Rev. B **57**, 12229–12233 (1998).
- ¹²⁸T. Sota and K. Suzuki, "Phonon attenuation in heavily doped many-valley semiconductors," J. Phys. C **15**, 6991–7002 (1982).
- ¹²⁹Y. Quan, S. Yue, and B. Liao, "Impact of electron-phonon interaction on thermal transport: A review," Nanoscale Microscale Thermophys. Eng. **25**, 73–90 (2021).
- ¹³⁰N. H. Protik, C. Li, M. Pruneda, D. Broido, and P. Ordejón, "The elphbolt ab initio solver for the coupled electron-phonon Boltzmann transport equations," npj Comput. Mater. **8**, 28 (2022).
- ¹³¹J. Zhou, B. Liao, B. Qiu, S. Huberman, K. Esfarjani, M. S. Dresselhaus, and G. Chen, "Ab initio optimization of phonon drag effect for lower-temperature thermoelectric energy conversion," Proc. Nat. Acad. Sci. U.S.A. **112**, 14777–14782 (2015).
- ¹³²M. Fiorentini and N. Bonini, "Thermoelectric coefficients of *n*-doped silicon from first principles via the solution of the Boltzmann transport equation," Phys. Rev. B **94**, 085204 (2016).
- ¹³³L. J. Challis and L. Halbo, "Evidence for a Jahn-Teller effect in *p*-Ge from magnetothermal conductivity measurements," Phys. Rev. Lett. **28**, 816–819 (1972).
- ¹³⁴L. J. Challis, S. C. Haseler, and A. Ramdane, "The magnetothermal conductivity of *p*-type germanium," J. Phys. C **11**, 4695–4706 (1978).
- ¹³⁵L. J. Challis and S. C. Haseler, "The effect of uniaxial stress on the thermal conductivity of *p*-Ge," J. Phys. C **11**, 4681–4694 (1978).
- ¹³⁶C. Claeys and E. Simoen, "Basic radiation damage mechanisms in semiconductor materials and devices," in *Radiation Effects in Advanced Semiconductor Materials and Devices* (Springer, Berlin, 2002), pp. 9–52.
- ¹³⁷H. J. Albany and M. Vandevyver, "Low-temperature thermal conductivity of fast-neutron-irradiated silicon and germanium," J. Appl. Phys. **38**, 425–430 (1967).
- ¹³⁸F. L. Vook, "Thermal conductivity of electron-irradiated germanium," Phys. Rev. **138**, A1234–A1241 (1965).
- ¹³⁹F. L. Vook, "Thermal conductivity of electron-irradiated silicon," Phys. Rev. **140**, A2014–A2019 (1965).
- ¹⁴⁰A. V. Inyushkin, A. N. Taldenkov, A. P. Yeliseyev, and V. G. Vins, "Thermal conductivity of type-Ib HPHT synthetic diamond irradiated with electrons," Diamond Relat. Mater. **139**, 110302 (2023).
- ¹⁴¹A. V. Inyushkin, A. N. Taldenkov, A. P. Yeliseyev, and V. G. Vins, personal communication (2023).
- ¹⁴²H. B. G. Casimir, "Note on the conduction of heat in crystals," Physica (Amsterdam) **5**, 495–500 (1938).
- ¹⁴³R. Berman, F. E. Simon, and J. M. Ziman, "The thermal conductivity of diamond at low temperatures," Proc. R. Soc. London, Ser. A **220**, 171–183 (1953).
- ¹⁴⁴R. Berman, E. L. Foster, and J. M. Ziman, "Thermal conduction in artificial sapphire crystals at low temperatures. I. Nearly perfect crystals," Proc. R. Soc. London, Ser. A **231**, 130–144 (1955).
- ¹⁴⁵A. K. McCurdy, H. J. Maris, and C. Elbaum, "Anisotropic heat conduction in cubic crystals in the boundary scattering regime," Phys. Rev. B **2**, 4077–4083 (1970).
- ¹⁴⁶J. M. Ziman, *Electrons and Phonons: The Theory of Transport Phenomena in Solids* (Clarendon Press, Oxford, 1960).
- ¹⁴⁷S. B. Soffer, "Statistical model for the size effect in electrical conduction," J. Appl. Phys. **38**, 1710–1715 (1967).
- ¹⁴⁸A. A. Maznev, "Boundary scattering of phonons: Specularity of a randomly rough surface in the small-perturbation limit," Phys. Rev. B **91**, 134306 (2015).
- ¹⁴⁹W. S. Hurst and D. R. Frankl, "Thermal conductivity of silicon in the boundary scattering regime," Phys. Rev. **186**, 801–810 (1969).
- ¹⁵⁰T. Klitsner and R. O. Pohl, "Phonon scattering at silicon crystal surfaces," Phys. Rev. B **36**, 6551–6565 (1987).
- ¹⁵¹J. W. Vandersande, "Boundary scattering in five natural type-IIa diamonds," Phys. Rev. B **13**, 4560–4567 (1976).
- ¹⁵²R. Berman and M. Martinez, "The thermal conductivity of diamonds," in *Diamond Research 1976. Supply to Indian Diamond Review* (Industrial Diamond Information Bureau, London, 1976), pp. 7–13.
- ¹⁵³V. Yurov, E. Bushuev, A. Bolshakov, E. Ashkinazi, I. Antonova, E. Zavedeev, A. Khomich, V. Voronov, and V. Ralchenko, "Etching kinetics of (100) single crystal diamond surfaces in a hydrogen microwave plasma, studied with *in situ* low-coherence interferometry," Phys. Status Solidi A **214**, 1700177 (2017).
- ¹⁵⁴D. G. Cahill, W. K. Ford, K. E. Goodson, G. D. Mahan, A. Majumdar, H. J. Maris, R. Merlin, and S. R. Phillpot, "Nanoscale thermal transport," J. Appl. Phys. **93**, 793–818 (2002).
- ¹⁵⁵D. G. Cahill, P. V. Braun, G. Chen, D. R. Clarke, S. Fan, K. E. Goodson, P. Kebbinski, W. P. King, G. D. Mahan, A. Majumdar, H. J. Maris, S. R. Phillpot, E. Pop, and L. Shi, "Nanoscale thermal transport. II. 2003–2012," Appl. Phys. Rev. **1**, 011305 (2014).
- ¹⁵⁶W. Liu and M. Asheghi, "Phonon-boundary scattering in ultrathin single-crystal silicon layers," Appl. Phys. Lett. **84**, 3819–3821 (2004).
- ¹⁵⁷A. M. Marconnet, M. Asheghi, and K. E. Goodson, "From the Casimir limit to phononic crystals: 20 years of phonon transport studies using silicon-on-insulator technology," J. Heat Transfer **135**, 061601 (2013).
- ¹⁵⁸P. Jiang, L. Lindsay, X. Huang, and Y. K. Koh, "Interfacial phonon scattering and transmission loss in >1 μm thick silicon-on-insulator thin films," Phys. Rev. B **97**, 195308 (2018).
- ¹⁵⁹L. Sang, "Diamond as the heat spreader for the thermal dissipation of GaN-based electronic devices," Funct. Diam. **1**, 174–188 (2021).
- ¹⁶⁰G. Aiello, T. Scherer, K. Avramidis, N. Casal, T. Franke, M. Gagliardi, G. Ganzenbein, M. Henderson, J. Jelonnek, A. Meier, G. Saibene, S. Schreck, D. Strauss, M. Thumm, M. Q. Tran, C. Wild, and E. Woerner, "Diamond window technology for electron cyclotron heating and current drive: State of the art," Fusion Sci. Technol. **75**, 719–729 (2019).
- ¹⁶¹H. A. Atikian, N. Sinclair, P. Latawiec, X. Xiong, S. Meesala, S. Gauthier, D. Wintz, J. Randi, D. Bernot, S. DeFrances, J. Thomas, M. Roman, S. Durrant, F. Capasso, and M. Lončar, "Diamond mirrors for high-power continuous-wave lasers," Nat. Commun. **13**, 2610 (2022).
- ¹⁶²J. E. Graebner, S. Jin, G. W. Kammlott, J. A. Herb, and C. F. Gardiner, "Large anisotropic thermal conductivity in synthetic diamond films," Nature **359**, 401–403 (1992).
- ¹⁶³R. B. Simon, J. Anaya, F. Faili, R. Balmer, G. T. Williams, D. J. Twitchen, and M. Kuball, "Effect of grain size of polycrystalline diamond on its heat spreading properties," Appl. Phys. Express **9**, 061302 (2016).
- ¹⁶⁴J. Anaya, T. Bai, Y. Wang, C. Li, M. Goorsky, T. L. Bouger, L. Yates, Z. Cheng, S. Graham, K. D. Hobart, T. I. Feygelson, M. J. Tadjer, T. J. Anderson, B. B. Pate, and M. Kuball, "Simultaneous determination of the lattice thermal conductivity and grain/grain thermal resistance in polycrystalline diamond," Acta Mater. **139**, 215–225 (2017).

- ¹⁶⁵A. V. Inyushkin, A. N. Taldenkov, V. G. Ralchenko, A. P. Bolshakov, and A. V. Khomich, "Isotope effect in thermal conductivity of polycrystalline CVD-diamond: Experiment and theory," *Crystals* **11**, 322 (2021).
- ¹⁶⁶P. G. Klemens, "Phonon scattering and thermal resistance due to grain boundaries," *Int. J. Thermophys.* **15**, 1345–1351 (1994).
- ¹⁶⁷A. V. Inyushkin, A. N. Taldenkov, V. G. Ral'chenko, V. I. Konov, A. V. Khomich, and R. A. Khmel'nitski, "Thermal conductivity of polycrystalline CVD-diamond: Experiment and theory," *J. Exp. Theor. Phys.* **107**, 462–472 (2008).
- ¹⁶⁸A. K. McCurdy, "Phonon conduction in elastically anisotropic cubic crystals," *Phys. Rev. B* **26**, 6971–6986 (1982).
- ¹⁶⁹I. G. Kuleyev, I. I. Kuleyev, S. M. Bakharev, and V. V. Ustinov, *Phonon Focusing and Phonon Transport*, Texts and Monographs in Theoretical Physics (De Gruyter, Berlin, 2020).
- ¹⁷⁰I. I. Kuleev, I. G. Kuleyev, S. M. Bakharev, and A. V. Inyushkin, "Effect of phonon focusing on the temperature dependence of thermal conductivity of silicon," *Phys. Status Solidi B* **251**, 991–1000 (2014).
- ¹⁷¹I. I. Kuleyev, I. G. Kuleyev, S. M. Bakharev, and A. V. Inyushkin, "Features of phonon transport in silicon rods and thin plates in the boundary scattering regime. The effect of phonon focusing at low temperatures," *Physica B* **416**, 81–87 (2013).
- ¹⁷²J. Vandersande, "Low temperature thermal conductivity of two natural diamonds: Anisotropic heat conduction in the boundary scattering regime," *J. Phys. (Paris) Colloq.* **39**, C6–1017–C6–1018 (1978).
- ¹⁷³J. A. Sussmann and A. Thellung, "Thermal conductivity of perfect dielectric crystals in the absence of Umklapp processes," *Proc. Phys. Soc.* **81**, 1122–1130 (1963).
- ¹⁷⁴R. N. Gurzhi, "Thermal conductivity of dielectrics and ferrodielectrics at low temperatures," *Sov. Phys. JETP* **19**, 490–493 (1964).
- ¹⁷⁵R. N. Gurzhi, "Hydrodynamic effects in solids at low temperature," *Sov. Phys. Usp.* **11**, 255–270 (1968).
- ¹⁷⁶R. A. Guyer and J. A. Krumhansl, "Thermal conductivity, second sound, and phonon hydrodynamic phenomena in nonmetallic crystals," *Phys. Rev.* **148**, 778–788 (1966).
- ¹⁷⁷L. P. Mezhov-Deglin, "Possibility of observing a Knudsen minimum in the thermal conductivity of insulator crystals," *Sov. Phys. Sol. St.* **22**, 1018–1021 (1980).
- ¹⁷⁸G. A. Armstrong, A. A. Helmy, and A. S. Greenberg, "Boundary-limited thermal conductivity of hcp ^4He ," *Phys. Rev. B* **20**, 1061–1064 (1979).
- ¹⁷⁹L. P. Mezhov-Deglin, "Thermal conductivity of solid He-4," *Sov. Phys. JETP* **19**, 1297–1298 (1964); "Measurement of the thermal conductivity of crystalline He4," *Sov. Phys. JETP* **22**, 47–56 (1966); "Influence of dimensions on the thermal conductivity of crystalline He4 samples," *Sov. Phys. JETP* **25**, 568–571 (1967).
- ¹⁸⁰W. D. Seward, D. Lazarus, and S. C. Fain, "Thermal conductivity of hexagonal close-packed solid helium four at high densities," *Phys. Rev.* **178**, 345–355 (1969).
- ¹⁸¹E. M. Hogan, R. A. Guyer, and H. A. Fairbank, "Thermal conductivity of oriented single crystals of hexagonal close-packed helium 4," *Phys. Rev.* **185**, 356–373 (1969).
- ¹⁸²W. C. Thomlinson, "Evidence for anomalous phonon excitations in solid He^3 ," *Phys. Rev. Lett.* **23**, 1330–1332 (1969).
- ¹⁸³V. N. Kopylov and L. P. Mezhov-Deglin, "Investigation of the kinetic coefficients of bismuth at helium temperatures," *Sov. Phys. JETP* **38**, 357–364 (1974).
- ¹⁸⁴L. P. Mezhov-Deglin, V. N. Kopylov, and E. S. Medvedev, "Contributions of various phonon relaxation mechanisms to the thermal resistance of the crystal lattice of bismuth at temperatures below 2 K," *Sov. Phys. JETP* **40**, 557–563 (1975).
- ¹⁸⁵Z. Ding, J. Zhou, B. Song, V. Chiloyan, M. Li, T.-H. Liu, and G. Chen, "Phonon hydrodynamic heat conduction and Knudsen minimum in graphite," *Nano Lett.* **18**, 638–649 (2018).
- ¹⁸⁶X. Huang, Y. Guo, Y. Wu, S. Masubuchi, K. Watanabe, T. Taniguchi, Z. Zhang, S. Volz, T. Machida, and M. Nomura, "Observation of phonon Poiseuille flow in isotopically purified graphite ribbons," *Nat. Commun.* **14**, 2044 (2023).
- ¹⁸⁷S. Lee, D. Broido, K. Esfarjani, and G. Chen, "Hydrodynamic phonon transport in suspended graphene," *Nat. Commun.* **6**, 6290 (2015).
- ¹⁸⁸K. Ghosh, A. Kusiak, and J.-L. Battaglia, "Phonon hydrodynamics in crystalline materials," *J. Phys.: Condens. Matter* **34**, 323001 (2022).
- ¹⁸⁹X. Li, H. Lee, E. Ou, S. Lee, and L. Shi, "Reexamination of hydrodynamic phonon transport in thin graphite," *J. Appl. Phys.* **131**, 075104 (2022).
- ¹⁹⁰A. Gibin, G. G. Devyatkh, A. V. Gusev, R. K. Kremer, M. Cardona, and H.-J. Pohl, "Heat capacity of isotopically enriched ^{28}Si , ^{29}Si and ^{30}Si in the temperature range $4\text{ K} < T < 100\text{ K}$," *Solid State Commun.* **133**, 569–572 (2005).
- ¹⁹¹P. D. Desai, "Thermodynamic properties of iron and silicon," *J. Phys. Chem. Ref. Data* **15**, 967–983 (1986).